

---

# CMS Physics Analysis Summary

---

Contact: cms-pag-conveners-susy@cern.ch

2017/03/21

## Search for electroweak production of charginos and neutralinos in multilepton final states in pp collision data at $\sqrt{s} = 13$ TeV

The CMS Collaboration

### Abstract

Searches are presented for direct electroweak production of charginos and neutralinos in signatures with two light leptons of the same charge and with three or more leptons including up to two hadronically decaying  $\tau$  leptons. The results are based on a sample of proton-proton collision data collected at a center-of-mass energy  $\sqrt{s} = 13$  TeV recorded with the CMS detector, corresponding to an integrated luminosity of  $35.9 \text{ fb}^{-1}$ . The observed event rates are in agreement with expectations from the standard model. These results probe charginos and neutralinos with masses up to values between 225 and 1150 GeV, depending on the model parameters assumed. These results significantly extend the phase space probed with previous searches.



## 1 Introduction

The standard model (SM) of particle physics is a very successful and coherent theory that describes the vast majority of the particle physics phenomena. So far it has withstood a multitude of challenges from precision measurements. Searches for new physics beyond the SM carried by various experiments also have not revealed a convincing evidence for the existence of beyond the SM phenomena. A recent triumph of the SM is the 2012 discovery of a Higgs boson ( $H$ ) by the ATLAS and CMS Collaborations at the CERN LHC [1–3]. Despite the success, the SM suffers from several shortcomings, such as the absence of a dark matter candidate and the hierarchy problem, which requires fine-tuned suppression of large quantum corrections to keep the Higgs boson mass at the electroweak scale. Supersymmetry (SUSY) [4–12] is an extension of the SM that introduces an additional symmetry between bosons and fermions, and provides superpartners to the SM particles. This extension offers a solution to several problems of the SM, including those cited above. In particular, in the case of conserved  $R$ -parity [9], SUSY particles are created in pairs. Thus the lightest SUSY particle (LSP) is stable, making it a possible dark-matter candidate. Furthermore, the existence of not too heavy superpartners leads to a cancellation of the large quantum corrections to the Higgs boson mass without large fine tuning.

Searches for new physics in the SUSY context constitute a major part of the LHC physics program. While no evidence of such new particles has been found with the samples of proton-proton (pp) collision data collected at  $\sqrt{s} = 7$  and 8 TeV, stringent constraints have been placed on the masses of the colored superpartners (squarks and gluinos) ranging from several hundreds of GeV to about 1.5 TeV, depending on the assumptions entering into the models for the interpretation of the results [13, 14]. On the other hand, the cross sections associated with electroweak production of SUSY particles are far lower than those for strong production. This directly translates into significantly lower exclusion limits, ranging from about 100 GeV to 700 GeV [15–17], on the masses of sparticles produced exclusively via the electroweak interaction. This production mechanism of sparticles becomes dominant in case colored superpartners are too heavy to be produced.

In 2015, an increase in the LHC centre-of-mass energy to 13 TeV led to a significant increase in the anticipated production cross section for particles with masses of order 1 TeV. As a consequence of this, the reach of searches for strongly coupled new particles already surpassed the results of the previous LHC run with the data collected in 2015 corresponding to an integrated luminosity of  $2.3 \text{ fb}^{-1}$  at the CMS detector and of  $3.2 \text{ fb}^{-1}$  at the ATLAS detector, allowing to probe gluinos with masses up to 1.7 TeV [18–24]. As the increase in pair production cross section of charginos and neutralinos in the mass range from 200 to 600 GeV is only a factor 2 to 4. A search for new particles produced via the electroweak interaction at  $\sqrt{s} = 13 \text{ TeV}$  using the full 2016 dataset, is presented in this document.

This note describes a search for direct production of charginos and neutralinos decaying to final states with two (same-sign), three or more charged leptons (with up to two  $\tau_h$ ), little hadronic activity and significant missing transverse momentum ( $E_T^{\text{miss}}$ ). We use a data sample of pp collisions recorded during 2016 with the CMS detector which corresponds to an integrated luminosity of  $35.9 \text{ fb}^{-1}$ . Similar searches have been reported by the CMS and ATLAS collaborations during LHC Run I [15–17] and Run II [25, 26].

This note is organized as follows: after a brief description of the targeted SUSY models (Section 2) and the detector (Section 3), we describe the event selection in Section 4 and the search strategy in Section 5. Section 6 covers the background estimation of the SM processes contributing to our signal regions. In Section 7 we report on the systematic uncertainties affecting

the search. In Section 8 we present the results and in Section 9 we discuss the interpretations of these results in the context of the different SUSY scenarios considered. Finally, Section 10 summarizes the conclusions of this search.

## 2 SUSY models

This search targets different scenarios of direct electroweak production of charginos  $\tilde{\chi}_1^\pm$  and neutralinos  $\tilde{\chi}_2^0$ , which decay into final states containing two, three or four charged leptons ( $e^\pm, \mu^\pm, \tau^\pm$ ), in the context of simplified models [27]. In such models, the masses and the decay modes of the relevant particles are the only free parameters. The  $\tilde{\chi}_1^\pm$  and  $\tilde{\chi}_2^0$  are set to be wino-like and mass degenerate and the  $\tilde{\chi}_1^0$  is set to be bino-like.

### $\tilde{\chi}_1^\pm \tilde{\chi}_2^0$ production with light sleptons

In the first scenario considered, the charginos and neutralinos decay to leptons via intermediate sleptons or sneutrinos, the SUSY partners of leptons and neutrinos, as shown in Fig. 1. The combination of gauge eigenstates making up the neutralinos and charginos, and their masses, will determine whether their decays through sleptons and sneutrinos (that are assumed to be mass-degenerate) lead to all three lepton flavors with equal probability (flavor-democratic model), or if they prefer to decay to  $\tau$  leptons. Three different scenarios for the decays are considered:

- **$\tilde{\chi}_1^\pm \tilde{\chi}_2^0$  production with  $\tilde{\ell}_L$ -mediated decays:** The chargino/neutralino decay via sleptons or sneutrinos to all lepton flavors with the same branching fraction (“flavor-democratic” scenario). As the decay through sleptons or sneutrinos happens with equal probability, only 50% of the decays will lead to three-lepton final states.
- **$\tilde{\chi}_1^\pm \tilde{\chi}_2^0$  production with  $\tilde{\ell}_R$ -mediated decays:** The chargino decays only to a  $\tau$  lepton (“ $\tau$ -enriched” scenario), as expected for right-handed sleptons, while the neutralino still decays to all three flavors. Sneutrinos are considered to be heavy and decoupled and do not participate in this process.
- **$\tilde{\chi}_1^\pm \tilde{\chi}_2^0$  production with  $\tilde{\tau}$ -mediated decays:** The first- and second-generation sleptons and sneutrinos are too heavy and the chargino/neutralino only decays via a  $\tilde{\tau}$ . We will refer to this model as the “ $\tau$ -dominated” scenario. Sneutrinos are considered to be heavy and decoupled and do not participate in this process.

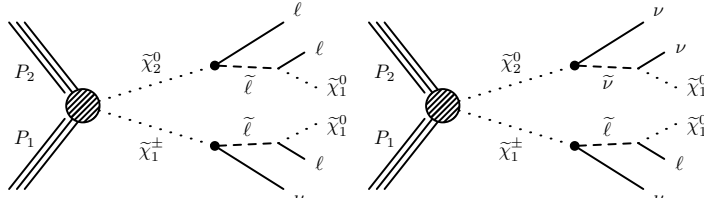


Figure 1: Chargino-neutralino pair production with decays mediated by sleptons and sneutrinos, leading to a three-lepton final state.

In these simplified models, the slepton mass is assumed to lie between the  $\tilde{\chi}_1^\pm / \tilde{\chi}_2^0$  and the  $\tilde{\chi}_1^0$ , and the branching fraction to leptons is taken to be 100%. Three different mass assumptions are considered:  $m_{\tilde{\ell}} = m_{\tilde{\nu}} = m_{\tilde{\chi}_1^0} + x \cdot (m_{\tilde{\chi}_2^0} - m_{\tilde{\chi}_1^0})$ , with  $x = 0.05, 0.5$  and  $0.95$ . For the two extreme cases one of the three leptons is very soft and may escape detection. A same-sign final state is used in these cases to recover some of these lost events without the penalty of increasing the SM background.

## $\tilde{\chi}_1^\pm \tilde{\chi}_2^0$ production with heavy sleptons

In the second scenario, we assume that the sleptons are too heavy and that the  $\tilde{\chi}_1^\pm / \tilde{\chi}_2^0$  undergo a direct decay to the lightest SUSY particle (LSP) via the emission of a  $W$ ,  $Z$ , or Higgs boson as depicted in Fig. 2. The chargino decays to a  $W$  and the  $\tilde{\chi}_1^0$ , while the neutralino can decay either to a  $Z$  or  $H$  boson and the  $\tilde{\chi}_1^0$ . Here, “ $H$ ” refers to the 125 GeV SM Higgs boson that is the lightest CP-even state of an extended Higgs sector. The observation of such a SUSY-like process involving a Higgs boson would provide evidence that SUSY particles couple to the Higgs field. The  $H$  boson is expected to have SM properties if all the other Higgs bosons are much heavier [12]. If the Higgs boson decays to  $WW$ ,  $ZZ$  or  $\tau\tau$ , which would further decay leptonically, one can expect multiple leptons in the final state. However, compared to the other models included in this analysis, the leptonic branching fractions are rather small.

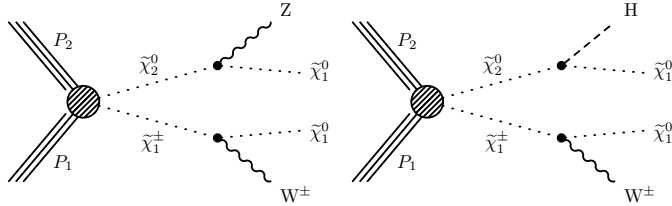


Figure 2: Chargino-neutralino pair production with the chargino decaying to  $W$  and the LSP and the neutralino decaying to (left) a  $Z$  boson and the LSP or (right) a  $H$  boson and the LSP.

## 3 The CMS detector

The central feature of the CMS apparatus is a superconducting solenoid of 6 m internal diameter, providing a magnetic field of 3.8 T. Within the superconducting solenoid volume are a silicon pixel and strip tracker, a lead tungstate crystal electromagnetic calorimeter (ECAL), and a brass and scintillator hadron calorimeter (HCAL), each composed of a barrel and two endcap sections. Forward calorimeters extend the pseudorapidity [28] coverage provided by the barrel and endcap detectors. Muons are measured in gas-ionization detectors embedded in the steel flux-return yoke outside the solenoid. The first level of the CMS trigger system, composed of custom hardware processors, uses information from the calorimeters and muon detectors to select the most interesting events in a fixed time interval of less than 4  $\mu$ s. The high-level trigger processor farm further decreases the event rate from around 100 kHz to around 1 kHz, before data storage. A more detailed description of the CMS detector, together with a definition of the coordinate system used and the relevant kinematic variables, can be found in Ref. [28].

## 4 Event selection and Monte Carlo simulation

The events are recorded if they satisfy the requirements of the CMS two-level trigger system. As we consider different lepton multiplicities in the final state a combination of several trigger paths is required to cover all possible cases and maximize acceptance. Events with at least two light leptons rely mostly on dilepton triggers with very loose isolation requirements and transverse momentum ( $p_T$ ) greater than 17 (23) GeV for the leading and  $p_T > 8$  (12) GeV for the sub-leading muon (electron). Single lepton triggers are used to increase the acceptance. For the final state with two hadronic taus ( $\tau_h$ ) and one electron or muon we use single lepton triggers requiring an isolated  $\mu$  (e) with  $p_T > 24$  (27) GeV. Typical trigger efficiencies for leptons satisfying the offline selection criteria described below are 98% (92%) per electron (muon), and 96%

per  $\tau_h$ . In final states with three or more leptons, the total trigger efficiency is close to 100% because of the multiple dilepton combinations.

In the offline analysis, the information from all subdetectors is combined by the CMS particle-flow (PF) algorithm [29, 30] to reconstruct and identify individual particles and to provide a global interpretation of the event. The particles are classified into charged hadrons, neutral hadrons, photons, electrons, and muons.

We require electrons to have  $|\eta| < 2.5$ , to ensure that they are within the tracking volume, and a minimum  $p_T$  of 10 GeV. The electron identification is performed using a multivariate discriminant built from variables that characterize the shower shape and track quality. To reject electrons from photon conversions, we reject candidates that have missing hits in the innermost layers of the tracking system or are matched to a secondary conversion vertex candidate [31].

Muon candidates are reconstructed by combining the information from the silicon tracker and the muon spectrometer in a global fit [32]. An identification selection is performed using the quality of the geometrical matching between the tracker and the muon system measurements. Only muons within the muon system acceptance  $|\eta| < 2.4$  and a minimum  $p_T$  of 10 GeV are considered.

Lepton candidates (electrons and muons) are required to be consistent with originating from the primary vertex, that is, the collision vertex for which the summed  $p_T^2$  of the associated tracks is the largest. The transverse  $d_0$  (longitudinal  $d_z$ ) impact parameter of the leptons must not exceed 0.5 (1.0) mm with respect to this vertex, they must satisfy a requirement on the impact parameter significance  $SIP_{3D} \equiv |d_{3D}|/\sigma(d_{3D}) < 8$ , where  $d_{3D}$  is the three-dimensional impact parameter with respect to the vertex and  $\sigma(d_{3D})$  is its uncertainty, as estimated from the track fit. Furthermore, leptons are required to be locally isolated. An isolation variable  $I_{\text{mini}}$  [33, 34] is computed as the ratio of the scalar  $p_T$  sum of charged hadrons, neutral hadrons, and photons within a cone around the lepton candidate direction at the vertex, to the transverse momentum  $p_T(\ell)$  of the lepton candidate. The cone radius  $\Delta R$  depends on  $p_T(\ell)$  as:

$$\Delta R(p_T(\ell)) = \frac{10 \text{ GeV}}{\min [\max(p_T(\ell), 50 \text{ GeV}), 200 \text{ GeV}]} \quad (1)$$

The varying isolation cone definition takes into account the increased collimation of the decay products of a hadron as its  $p_T$  increases, and it reduces the inefficiency from accidental overlap between the lepton and other objects in an event. Loosely isolated leptons are required to have  $I_{\text{mini}} < 0.4$ . Electrons and muons that pass all the aforementioned requirements are referred to as *loose* in this analysis.

In order to discriminate between leptons originating from decays of heavy particles such as W and Z bosons or SUSY particles (“prompt” leptons) and those produced in hadron decays or in photon conversions as well as misidentified hadrons (“nonprompt” leptons), we use a multivariate discriminator based on a boosted decision tree (BDT) [35, 36] that takes as an input the following variables: vertex variables such as  $d_0$ ,  $d_z$ ,  $SIP_{3D}$ ,  $I_{\text{mini}}$ , variables related to the jet closest to the lepton, such as the ratio between the  $p_T$  of the lepton and the  $p_T$  of the jet ( $p_T^{\text{ratio}}$ ), the b-tagging discriminator value of the jet, the number of charged particles in the jet, and the  $p_T^{\text{rel}}$  variable [34] and other identification variables such as the muon segment compatibility and the electron identification multivariate discriminant. The BDT is trained in simulation with prompt leptons from  $t\bar{t}Z$  and with nonprompt leptons from  $t\bar{t}$ . Leptons satisfying a requirement of this discriminant having fulfilled the loose requirements are referred as *tight* leptons. Two working points are defined, one with higher efficiency for the three or more lepton channel

and one with high nonprompt background rejection for the same-sign dilepton channel. The identification efficiency for electrons passing tight criteria is varying between 20% for the low- $p_T$  leptons in the endcap regions, and 90% for high- $p_T$  leptons; while for muons it is between 82% and 100% depending on muon  $p_T$ .

The  $\tau_h$  candidates are reconstructed with the hadron-plus-strips algorithm [37]. They are required to pass the “decay mode finding” discriminator, selecting one- or three-prong decay modes, with or without additional  $\pi^0$  particles. In addition, they must fulfill  $p_T > 20\text{ GeV}$ ,  $|\eta| < 2.3$ , and isolation requirements in a  $\Delta R = \sqrt{(\Delta\eta)^2 + (\Delta\phi)^2} = 0.5$  cone. The typical  $\tau_h$  identification efficiency of these selection requirements is 50% while the jet misidentification rate is well below 0.1% [38].

Particle-flow candidates are clustered into jets using the anti- $k_t$  algorithm [39] with a distance parameter of 0.4, as implemented in the FASTJET package [40, 41]. Jets are required to satisfy quality requirements [42] to remove those likely arising from anomalous energy deposits. Charged hadrons are not considered if they do not originate from the selected primary vertex. After the estimated contribution of neutral particles from additional pp interactions (pileup) is subtracted by using the average amount of transverse energy in the event per unit area [43, 44], jet energies are corrected for residual nonuniformity and nonlinearity of the detector response using simulation and data [45]. Only jets with  $p_T > 25\text{ GeV}$ ,  $|\eta| < 2.4$  and separated from any lepton candidate by  $\Delta R > 0.4$  are retained.

To identify jets originating from b quarks, the combined secondary vertex algorithm CSVv2 [46, 47] is used. Jets with  $p_T > 25\text{ GeV}$  and  $|\eta| < 2.4$  are considered b quark jets (“b jets”) if they satisfy the requirements of the medium working point [46, 47] of the algorithm. These requirements result in an efficiency of approximately 70% for tagging a b quark jet, and a mistagging rate of 1.5% for light-quark and gluon jets, as measured in  $t\bar{t}$  events. Simulated events are corrected for differences in the performance of the algorithm between data and simulation. Events with at least one identified b jet are vetoed in the analysis to reduce the  $t\bar{t}$  background.

No requirements on the number of jets in an event are imposed for the three- and four-lepton search regions, other than the b jet veto discussed above. For the two-lepton search we consider events in which the leptons are accompanied by zero and by one jet with  $p_T > 40\text{ GeV}$ .

The  $E_T^{\text{miss}}$  is obtained as the magnitude of the negative vector sum  $\vec{p}_T^{\text{miss}}$  of the transverse momenta of all reconstructed PF candidates and is further adjusted to account for jet energy corrections applied to the event [48].

Monte Carlo (MC) simulated samples, which include the effects of pileup, are used to estimate the background from SM processes with prompt leptons (see Section 6) and to calculate the selection efficiency for various new-physics scenarios. The SM background samples are produced with the MADGRAPH5\_AMC@NLO v2.3.3 generator [49] at leading order (LO) or next-to-leading order (NLO) accuracy in perturbative quantum chromodynamics, including up to one or two additional partons in the matrix element calculations. The exception is the diboson samples which are produced with the POWHEG v2 [50, 51] generator without additional partons in the matrix element calculations. The NNPDF3.0LO [52] parton distribution functions (PDFs) are used for the simulated samples generated at LO and the NNPDF3.0NLO [52] PDFs for those generated at NLO. Parton showering and hadronization are described using the PYTHIA 8.205 generator [53] with the CUETP8M1 tune [54, 55]. The CMS detector response for the background samples is modeled with the GEANT4 package [56].

Signal samples are generated with MADGRAPH5\_AMC@NLO at LO precision, including up to two additional partons in the matrix element calculations; Parton showering and hadronization

as well as decays of SUSY particles are modelled with PYTHIA, while the detector simulation is performed with the CMS fast simulation package [57]. Any residual differences in the detector response description between the GEANT4 and fast simulations are corrected for, with corresponding uncertainties on the signal acceptance taken into account.

## 5 Search strategy

This search is designed to target several scenarios described in Section 2 of direct electroweak production of charginos  $\tilde{\chi}_1^\pm$  and neutralinos  $\tilde{\chi}_2^0$  leading to final states with two, three or four leptons and little hadronic activity. The specific strategy of the analysis is guided by the assumption that  $R$ -parity is conserved, hence leading to the presence of particles in the final states that evade detection, yielding a sizable  $E_T^{\text{miss}}$ .

The small cross-section of the electroweak production challenges the analysis design, which includes all the possible final states to enhance the discovery potential. Therefore, the analysis is subdivided into several categories defined by the number of leptons in the event, their flavor, and charge. Each of these categories is further subdivided into bins defined by the kinematic variables that allow to discriminate from the SM background contributions and increase the sensitivity to possible mass hierarchies of new particles.

Among the SM processes yielding the same final states as those targeted in this search there are: WZ production, nonprompt leptons, external and internal conversions, rare SM processes (i.e. multi-boson production or single boson production in association with a  $t\bar{t}$  pair) and charge misidentification. The dominant source of background varies depending on the considered category and thus the search strategy is tailored accordingly.

### 5.1 Two leptons same-sign category

Although the targeted models naturally yield three-lepton final states, for compressed scenarios one of the leptons from the decay chain of a neutralino can be very soft, such that it would not fulfill the selection requirements. However, requiring two same-sign leptons allows to recover some of these missing events while keeping the SM background under control.

Events with two same-sign leptons with  $p_T > 25$  (20) GeV for the leading and  $p_T > 15$  (10) GeV for the trailing electron (muon) and no third lepton passing the tight identification criteria defined before are considered into this category. In addition, events must have  $E_T^{\text{miss}} > 60$  GeV. To suppress the WZ background, events are vetoed if they contain an opposite-sign same-flavor (OSSF) pair formed from loose electrons or muons in a  $\pm 15$  GeV window around the Z boson mass. To reduce the contribution from the processes with low-mass resonances, events are vetoed if they contain an OSSF pair with an invariant mass below 12 GeV.

Events are first divided into two categories, with and without an initial-state radiation (ISR) jet ( $p_T > 40$  GeV) to increase the sensitivity to more compressed scenarios. The jet presence provides the final-state particles with a boost in the transverse plane and thus the potential for a moderate or large  $E_T^{\text{miss}}$ . Further binning is done in  $E_T^{\text{miss}}$ , the minimum transverse mass ( $M_T = \sqrt{2E_T^{\text{miss}}p_T^\ell(1 - \cos(\Delta\phi))}$ ) computed for each lepton, and the  $p_T$  of the dilepton system ( $p_T^{\ell\ell}$ ). The bins with enough statistics are also split by charge to help constraining some charge-asymmetric backgrounds.

Table 1: Search regions for events with two same-sign light flavor leptons.

$N_{\text{jets}}$	$M_{\text{T}}$ (GeV)	$p_{\text{T}}^{\ell\ell}$ (GeV)	$E_{\text{T}}^{\text{miss}} < 100 \text{ GeV}$	$100 \leq E_{\text{T}}^{\text{miss}} < 150 \text{ GeV}$	$150 \leq E_{\text{T}}^{\text{miss}} < 200 \text{ GeV}$	$E_{\text{T}}^{\text{miss}} \geq 200 \text{ GeV}$
0	< 100	< 50	SS 01	SS 02 (++)	SS 04	SS 05
				SS 03 (--)		
		> 50	SS 06	SS 07 (++)	SS 09	SS 10
		SS 08 (--)				
	> 100		SS 11	SS 12 (++)	SS 14	SS 15
				SS 13 (--)		
1	< 100	< 50	SS 16	SS 17 (++)	SS 19	SS 20
				SS 18 (--)		
		> 50	SS 21	SS 22 (++)	SS 24	SS 25
		SS 23 (--)				
	> 100		SS 26	SS 27 (++)	SS 29	SS 30
				SS 28 (--)		

## 5.2 Three or more leptons category

Most of the targeted models described in Section 2 and depicted in Figs. 1 and 2 yield three isolated leptons and significant  $E_{\text{T}}^{\text{miss}}$  in the final state.

Events are selected on the condition that they have  $E_{\text{T}}^{\text{miss}} > 50 \text{ GeV}$  and contain at least three leptons passing the identification criteria with a maximum of two  $\tau_h$ 's is allowed. The leading electron (muon) must satisfy  $p_{\text{T}} > 25$  (20) GeV, while the sub-leading electron (muon) must satisfy  $p_{\text{T}} > 15$  (10) GeV. These criteria originate from the  $p_{\text{T}}$  thresholds of the dilepton triggers used in the analysis. Moreover, in an event where a leading lepton is a muon, if the other leptons are electrons or taus, the leading muon is required to have  $p_{\text{T}} > 25 \text{ GeV}$ . For events with one e or  $\mu$  and two  $\tau_h$ , all leptons are additionally constrained to have  $|\eta| < 2.1$ , and the electron (muon) should have  $p_{\text{T}} > 30$  (25) GeV. These requirements are imposed to ensure that the selected events have high efficiency with the used triggers. To reduce the contribution from the processes with low-mass resonances, events are vetoed if they contain an OSSF pair with an invariant mass below 12 GeV. Additionally in events containing an OSSF pair of two e or  $\mu$ , the invariant mass of all three leptons is required not to be consistent with the mass of a Z boson ( $|M_{3\ell} - M_Z| > 15 \text{ GeV}$ ) in order to suppress contributions from asymmetric photon conversions.

These events are then classified according to the number of identified leptons and their flavor. We distinguish between final states with three and more than three leptons and between final states with and without hadronic taus as follows:

- Events with three light-flavor leptons (electrons or muons).
- Events with two light-flavor leptons and a  $\tau_h$ .
- Events with one light-flavor lepton and two  $\tau_h$ .
- Events with at least four light-flavor leptons and no  $\tau_h$ .
- Events with at least three light-flavor leptons and one  $\tau_h$ .
- Events with at least two light-flavor leptons and two  $\tau_h$ .

These categories are then further subdivided according to their kinematic properties to define the different search regions. Further binning of the events in the aforementioned categories is described in detail in the remainder of this Section.

### 5.2.1 Three light leptons (Signal regions A and B)

In most of the cases, two out of the three leptons (e or  $\mu$ ) will form an OSSF pair. For these events, we further divide the events into three bins of invariant mass of the dilepton pair,  $M_{\ell\ell}$

in order to separate processes that include a Z boson in the decay chain from processes where a Z boson is not involved. Two of the  $M_{\ell\ell}$  bins are defined to be above and below the Z mass, while the third one is defined as the Z mass window, and it is expected to contain the bulk of the standard model background events. In the case of three same-flavor leptons, the OSSF pair with the invariant mass closest to the mass of the Z-boson is used. The transverse mass  $M_T$  of the third lepton in the event is computed with respect to  $E_T^{\text{miss}}$ . Both variables,  $M_T$  and  $E_T^{\text{miss}}$ , are used to further categorize the events with most of the standard model background expected in low  $M_T$  and  $E_T^{\text{miss}}$  bins. These search regions, labelled as “A”, are summarized in Table 2.

Table 2: Search regions for events with three e or  $\mu$  that form at least one OSSF pair. Search region SR A15\* is contained within a control region of the analysis and is not used in the interpretation.

$M_T$ (GeV)	$E_T^{\text{miss}}$ (GeV)	$M_{\ell\ell} < 75$ GeV	$75 \leq M_{\ell\ell} < 105$ GeV	$M_{\ell\ell} \geq 105$ GeV
0 – 100	50 – 100	SR A01	3SR A15*	SR A32
	100 – 150	SR A02	SR A16	SR A33
	150 – 200	SR A03	SR A17	SR A34
	200 – 250	SR A04	SR A18	SR A35
	250 – 400	SR A05	SR A19	SR A36
	400 – 550		SR A20	
	$\geq 550$		SR A21	
100 – 160	50 – 100	SR A06	SR A22	SR A37
	100 – 150	SR A07	SR A23	SR A38
	150 – 200	SR A08	SR A24	SR A39
	$\geq 200$	SR A09	SR A25	SR A40
$\geq 160$	50 – 100	SR A10	SR A26	SR A41
	100 – 150	SR A11	SR A27	SR A42
	150 – 200	SR A12	SR A28	SR A43
	200 – 250	SR A13	SR A29	SR A44
	250 – 400	SR A14	SR A30	
	$\geq 400$		SR A31	

In the case that no OSSF pair is found, two bins each for  $M_{\ell\ell}$  and  $M_T$  are used. The low  $M_T$  bins are then further subdivided into two  $E_T^{\text{miss}}$  bins. Most of these events arise from a leptonic decay of  $Z \rightarrow \tau\tau$ , therefore, the  $M_{\ell\ell}$  is calculated from the opposite-sign (OS) dilepton pair whose invariant mass is closest to the mean dilepton mass determined from  $Z \rightarrow \tau\tau$  simulation, which is 50 GeV. If no OS pair is found, the event is assigned to the lowest  $M_{\ell\ell}$  bin, and the  $M_T$  is taken to be the minimum  $M_T$  calculated from any of the three lepton and the  $E_T^{\text{miss}}$ . These search regions, labelled as “B”, are summarized in Table 3.

Table 3: Search regions for events with three e or  $\mu$  that do not form an OSSF pair.

$M_T$ (GeV)	$E_T^{\text{miss}}$ (GeV)	$M_{\ell\ell} < 100$ GeV	$M_{\ell\ell} \geq 100$ GeV
0 – 120	50 – 100	SR B01	SR B04
	$> 100$	SR B02	SR B05
	$> 120$	SR B03	SR B06

### 5.2.2 Three leptons with at least one $\tau_h$ (Signal regions C to F)

A third category is built with events with two e or  $\mu$  forming an OSSF pair and a  $\tau_h$ ; it uses the same three  $M_{\ell\ell}$  bins as in category A, again with the goal to separate off-Z and on-Z regions. For all events with a  $\tau_h$ ,  $M_{T2}$  [58, 59] replaces  $M_T$  for the further subdivision of the bins, as  $M_{T2}$  is found to be a more powerful discriminator with respect to the  $t\bar{t}$  background. The two-lepton transverse  $M_{T2}$  is computed as

$$M_{T2}^2 = \min_{\vec{p}_{T1}^{\text{miss}} + \vec{p}_{T2}^{\text{miss}} = \vec{p}_T^{\text{miss}}} \left[ \max \{ M_T^2(\vec{p}_T^{\ell_1}, \vec{p}_{T1}^{\text{miss}}), M_T^2(\vec{p}_T^{\ell_2}, \vec{p}_{T2}^{\text{miss}}) \} \right], \quad (2)$$

where the minimization is done over all possible momenta  $\vec{p}_{T1}^{\text{miss}}$  and  $\vec{p}_{T2}^{\text{miss}}$  summing to the observed  $\vec{p}_T^{\text{miss}}$  in sum. The probability to misidentify  $\tau_h$  is significantly larger than that to misidentify an electron or muon, hence  $M_{T2}$  is computed with a pair of light leptons in this category. The  $M_{T2}$  bins are divided so that the vast majority of the SM backgrounds are at low  $M_{T2}$ , especially the  $t\bar{t}$  contribution. For the search regions containing a  $Z$  candidate, the categorization in terms of  $M_{T2}$  is not performed. The complete set of cuts defining the signal regions for events in this category “C” is given in Table 4.

For events with a  $\tau_h$  and two light leptons that do not form an OSSF pair (i.e.  $e^\pm e^\pm, \mu^\pm \mu^\pm, \mu^\pm e^\mp$ ), the OS pair, if present, with the invariant mass closest to the corresponding dilepton mass expected from a  $Z \rightarrow \tau\tau$  decay (50 GeV for  $e\mu$  and 60 GeV for  $e\tau_h$  or  $\mu\tau_h$ ) is used for the event categorization. If no OS pair is present, the event is counted in the lowest  $M_{\ell\ell}$  bin. In this case, further categorization is performed depending on whether the  $e$  or  $\mu$  form an OS (category “D”) or SS (category “E”) pair. The final search region binning is shown in Table 5 and 6. The  $M_{T2}$  variable is computed with a pair of the opposite-sign light leptons if it is present, otherwise with a light lepton leading in  $p_T$  and a  $\tau_h$ .

The last category (category “F”) includes events with two  $\tau_h$ ’s and an  $e$  or  $\mu$ , for which the binning is shown in Table 7. The  $M_{T2}$  variable is computed with the light lepton and the leading  $\tau_h$ .

Table 4: Search region definition for events with two  $e$  or  $\mu$  forming an OSSF pair and one  $\tau_h$  candidate. Regions where there is a  $Z$  boson candidate are not split into  $M_{T2}$  categories.

$E_T^{\text{miss}}$ (GeV)	$75 \leq M_{\ell\ell} < 105$ GeV	$M_{T2}(\ell_1, \ell_2)$ (GeV)	$M_{\ell\ell} < 75$ GeV	$M_{\ell\ell} \geq 105$ GeV
50 – 100	SR C06	0 – 100	SR C01	SR C12
100 – 150	SR C07		SR C02	SR C13
150 – 200	SR C08		SR C03	SR C14
200 – 250	SR C09		SR C04	SR C15
250 – 300			SR C05	SR C16
300 – 400	SR C10			
$\geq 400$	SR C11			
50 – 200		$\geq 100$	SR C17	
$\geq 200$			SR C18	

Table 5: Search region definition for events with one  $e$  and one  $\mu$  of opposite sign, and one  $\tau_h$  candidate.

$M_{T2}(\ell_1, \ell_2)$ (GeV)	$E_T^{\text{miss}}$ (GeV)	$M_{\ell\ell} < 60$ GeV	$60 \leq M_{\ell\ell} < 100$ GeV	$M_{\ell\ell} \geq 100$ GeV
0 – 100	50 – 100	SR D01	SR D06	SR D11
	100 – 150	SR D02	SR D07	SR D12
	150 – 200	SR D03	SR D08	SR D13
	200 – 250	SR D04	SR D09	SR D14
	$\geq 250$	SR D05	SR D10	
$\geq 100$	50 – 200		SR D15	
	$\geq 200$		SR D16	

### 5.2.3 More than three leptons (Signal regions G to K)

The remaining search regions comprise of events with at least four leptons. This category benefits from much lower SM backgrounds compared to the three-lepton category, but suffers from low branching ratios.

Table 6: Search region definition for events with two  $e$  or  $\mu$  of same sign and one  $\tau_h$  candidate.

$M_{T2}(\ell_1, \tau)$ (GeV)	$E_T^{\text{miss}}$ (GeV)	$M_{\ell\ell} < 60$ GeV	$60 \leq M_{\ell\ell} < 100$ GeV	$M_{\ell\ell} \geq 100$ GeV
0 – 100	50 – 100	SR E01	SR E06	SR E11
	100 – 150	SR E02	SR E07	
	150 – 200	SR E03	SR E08	
	200 – 250	SR E04	SR E09	
	$\geq 250$	SR E05	SR E10	
	$\geq 100$	$\geq 50$		SR E12

Table 7: Search region definition for events with one electron or muon and two  $\tau_h$  candidates.

$M_{T2}(\ell, \tau_1)$ (GeV)	$E_T^{\text{miss}}$ (GeV)	$M_{\ell\ell} < 100$ GeV	$M_{\ell\ell} \geq 100$ GeV
0 – 100	50 – 100	SR F01	SR F07
	100 – 150	SR F02	SR F08
	150 – 200	SR F03	SR F09
	200 – 250	SR F04	SR F10
	250 – 300	SR F05	
	$\geq 300$	SR F06	
$\geq 100$	50 – 200		SR F11
	$\geq 200$		SR F12

The search regions are formed according to the number of OSSF pairs and the number of  $\tau_h$ 's in the event. This separation is motivated by the production of a Z or H boson in the decay chain, that would then decay into two light flavor leptons or two taus.

The data are further subdivided in intervals of  $E_T^{\text{miss}}$  with the goal to more efficiently discriminate between signal and background. The search region definitions and their notations are summarized in Table 8.

Table 8: Search region definition for events with four or more leptons.

$E_T^{\text{miss}}$ (GeV)	0 $\tau_h$		1 $\tau_h$		2 $\tau_h$	
	nOSSF $\geq 2$	nOSSF $< 2$	nOSSF $\geq 0$	nOSSF $\geq 2$	nOSSF $< 2$	
0 – 50	SR G01	SR H01	SR I01	SR J01	SR K01	SR K03
50 – 100	SR G02	SR H02	SR I02	SR J02	SR K02	
100 – 150	SR G03	SR H03	SR I03	SR J03		
150 – 200	SR G04	SR H04	SR I04	SR J04		
$\geq 200$	SR G05					

### 5.3 Aggregated signal regions

To facilitate the re-interpretation of these results, we provide a set of so-called “aggregated signal regions”. These regions are defined by a simpler selection that provides similar sensitivity to most of the signal models and phase space this analysis is targeting. The definition of all aggregated regions is summarized in Table 9.

## 6 Backgrounds

The SM backgrounds leading to the final states under consideration can be divided into the following categories:

- **WZ or  $W\gamma^*$  production:** When both W and  $Z(\gamma^*)$  bosons decay leptonically, these events produce the same signature as the new physics scenarios targeted by this analysis: three energetic and isolated leptons and a sizable  $E_T^{\text{miss}}$  due to a neutrino from the W boson decay. This is the dominant background by far in the searches with three e or  $\mu$  including an OSSF dilepton pair. The WZ process may also produce a same-sign dilepton signature when the Z boson is off-shell or when the  $\gamma^*$  boson is

Table 9: Definition of the aggregated regions for multilepton and two same-sign leptons final states.

nb	final state	definition
1	2 same-sign leptons	0 jets, $M_T > 100$ GeV and $E_T^{\text{miss}} > 140$ GeV
2	2 same-sign leptons	1 jets, $M_T < 100$ GeV, $p_T^{\ell\ell} < 100$ GeV and $E_T^{\text{miss}} > 200$ GeV
3	3 light leptons	$M_T > 120$ GeV and $E_T^{\text{miss}} > 200$ GeV
4	3 light leptons	$E_T^{\text{miss}} > 250$ GeV
5	2 light leptons and 1 tau	$M_{T2}(\ell_1, \tau) > 50$ GeV and $E_T^{\text{miss}} > 200$ GeV
6	1 light lepton and 2 taus	$M_{T2}(\ell, \tau_1) > 50$ GeV and $E_T^{\text{miss}} > 200$ GeV
7	1 light lepton and 2 taus	$E_T^{\text{miss}} > 75$ GeV
8	more than 3 leptons	$E_T^{\text{miss}} > 200$ GeV

produced, in which case one of the leptons from the  $Z(\gamma^*)$  boson decay may fail the applied selection criteria such as a  $Z$ -mass veto or a minimum  $p_T$  requirement on a vetoed lepton, or when the  $Z$  boson decays to  $\tau$  leptons yielding a semileptonic final state.

- **Nonprompt  $e$ ,  $\mu$ , and  $\tau_h$ :** Depending on the lepton multiplicity, this background is dominated by the  $W + \text{jets}$  (especially in the same-sign dilepton regions), or  $t\bar{t}$ , or Drell–Yan processes. This category provides the largest background contribution in the trilepton search regions without an OSSF pair, and those with a  $\tau_h$  candidate.
- **External and internal conversions:** These processes contribute to the same-sign dilepton or trilepton final state when a  $W$  or a  $Z$  boson radiates an initial- or final-state photon and this photon undergoes an asymmetric internal or external conversion in which one of the leptons has very low  $p_T$ . This soft lepton has a high probability of failing the selection criteria of the analysis, leading to a reconstructed two- (in case of a  $W$  boson) or three-lepton (in case of a  $Z$  boson) final state. This background mostly contributes to categories with an OSSF pair and to final states with two SS leptons.
- **Rare SM processes with multiple prompt leptons:** Rare SM processes that yield a SS lepton pair or three or more leptons include multiboson production ( $W$ ,  $Z$ ,  $H$ , or a prompt  $\gamma$ ), single-boson production in association with a  $t\bar{t}$  pair, and double parton scattering. Such processes generally have very small production rate and can in some cases be further suppressed by the  $b$  jet veto.
- **Charge misidentification:** A background from charge misidentification arises from events with an OS pair of isolated  $e\mu$  or  $ee$  in which the charge of one of the electrons is misreconstructed. In most cases, this arises from severe bremsstrahlung in the tracker material. This is a small background, manifesting itself in the same-sign dilepton category or in the category with a same-sign dilepton pair and a  $\tau_h$  candidate.

The  $WZ$  background contribution is normalized to data in a dedicated control region containing events with three light leptons: only events with an OSSF pair with an invariant mass of  $75 < M_{\ell\ell} < 105$  GeV are selected. Additional requirements on these events are:  $M_T < 100$  GeV and  $35 \text{ GeV} < E_T^{\text{miss}} < 100$  GeV. The purity of the  $WZ$  selection is approximately 86%. This definition overlaps with the search region SR A15 of the trilepton search category. As a consequence of the overlap with search region SR A15, the latter region is not used in the interpretation of the results in terms of new-physics models.

The tail of the  $M_T$  distribution is a result of, in order of importance, the accidental usage of a wrong pair of leptons to compute the mass of the  $Z$  candidate and the  $M_T$  of the  $W$  candidate (“mispairing” of the leptons), the different  $E_T^{\text{miss}}$  resolution in data compared to simulation, and the  $W$  width. The prediction of lepton mispairing in the simulation is confirmed in a control sample similar to the one described above but allowing only events with an OSSF pair of different flavor than the third lepton and using the opposite-sign pair of leptons of different flavor in  $M_{\ell\ell}$  computation. To estimate the effect of the different  $E_T^{\text{miss}}$  resolution and the  $W$  width on the  $W$  boson  $M_T$  distribution shape, we verify the  $M_T$  shape prediction of the simulation in  $W\gamma$  and  $W + \text{jets}$  control samples in data. After applying a high- $p_T$  threshold on the photon to suppress the contribution of  $W\gamma$  events produced by final-state radiation (FSR), we find the  $W$  boson  $M_T$  distribution shapes in the  $W\gamma$ ,  $W + \text{jets}$ , and  $WZ$  processes to be the same in simulation. We thus proceed to measure the  $W\gamma$  and  $W + \text{jets}$   $M_T$  shape in a dedicated control sample in which an energetic well identified and isolated photon with  $p_T > 50 \text{ GeV}$  is required, together with a lepton passing the same criteria as those selected in the trilepton search regions, and  $E_T^{\text{miss}} > 50 \text{ GeV}$ . A minimum separation of  $\Delta R > 0.3$  is required between the lepton and the photon to further reduce the FSR contribution. The residual  $W + \text{jets}$  contribution in this control sample constitutes about 20% of it, and it consists of events where a jet has very high electromagnetic fraction, and thus is not subject to large mismeasurements. After subtraction of the residual contamination from processes other than  $W\gamma$  or  $W + \text{jets}$ , the  $M_T$  shape measured in this control region is compared to the one predicted by the  $WZ$  simulation. The measured shape is found to agree well with the prediction from simulation within the statistical uncertainties, and the precision of this comparison is used to derive systematic uncertainties on the high- $M_T$  bins of the trilepton search.

The background from nonprompt light leptons is estimated using the “tight-to-loose” ratio method which is described in detail in Ref. [21]. The probability for a loosely defined light lepton to pass the full set of selection criteria is measured in a multijet sample in data enriched in nonprompt leptons, called the measurement region. Once measured, this probability is applied in a sample of events that pass the full kinematic selection, but where at least one of the leptons fails the nominal selection but passes the loose requirements, in order to predict the number of events from nonprompt leptons entering each search region. The contribution from nonprompt  $\tau_h$  leptons is estimated in a similar way. This time, the “tight-to-loose” ratio is measured in a  $Z + \text{jets}$  enriched control sample in data, in which a  $\tau_h$  candidate is required to be present in addition to an OSSF pair consistent with the  $Z$  boson decay. The residual contribution from prompt leptons in the measurement and application regions is subtracted using MC simulation. It is verified in both MC simulation and low- $E_T^{\text{miss}}$  data control regions that this method describes the background from the nonprompt leptons entering the different search regions within a systematic uncertainty of 30%.

The modeling of the conversion background is verified in a data control region enriched in both external and internal conversions. The rate of  $Z \rightarrow 2\ell$  with  $\gamma^{(*)} \rightarrow \ell\ell$ , where one of the leptons is out of acceptance is compared with the full prediction derived from the MC simulation and the nonprompt leptons estimation method, in an “off- $Z$ ” control region defined by  $|M_{\ell\ell} - M_Z| > 15 \text{ GeV}$ ,  $|M_{3\ell} - M_Z| < 15 \text{ GeV}$ , and  $E_T^{\text{miss}} < 50 \text{ GeV}$ . The predicted background yields are found to agree with the simulation within the statistical uncertainties. The scale factors derived for the modeling of the asymmetric conversions to electrons or muons in the  $Z\gamma^{(*)}$  process are found to be  $1.04 \pm 0.11$  and  $1.25 \pm 0.24$  respectively.

The charge misidentification background in the same-sign dilepton channel is estimated by reweighing the events with OS lepton pairs by the charge misidentification probability. For electrons, this probability is obtained from simulated  $t\bar{t}$  events and from an on- $Z$   $e^\pm e^\pm$  control

region in data, and it is in the range  $10^{-5}$ – $10^{-3}$  depending on the electron’s  $p_T$  and  $\eta$ . Studies of simulated events indicate that the muon charge misidentification probability is negligible. In the case of the same-sign dilepton +  $\tau_h$  final state, the charge misidentification background from WZ production and rare SM processes is taken directly from simulation and is not presented as a separate category.

## 7 Systematic uncertainties

The systematic uncertainties in the background estimates and signal acceptance affect both the overall normalization of the yields and the relative populations of processes in the search regions. The systematic uncertainties considered in this analysis are summarized in Table 10.

Experimental uncertainties include those in the lepton selection efficiency, the trigger efficiency, the jet energy scale, and the “b-tag veto” efficiency. Lepton identification and trigger efficiencies are computed with the “tag-and-probe” technique [31, 32], respectively, with an uncertainty of 3% per lepton. The  $\tau_h$  identification efficiency is determined within an uncertainty of 5% [38].

The total effect of the trigger efficiency and its uncertainty varies among the different search regions, being most important for the SS dilepton search, where it is estimated to be 3%. In the three- and four-lepton final states, the trigger efficiency is close to 100% due to the presence of one or two more leptons than required in the trigger, and the corresponding uncertainties in this efficiency are, respectively, 3 and 1%.

Table 10: Summary of systematic uncertainties in the event yields in the search regions. The upper group lists uncertainties related to experimental effects for all processes whose yield is estimated from simulation; the middle group lists uncertainties in these yields related to the event simulation process itself. The third group lists uncertainties for background processes whose yield is estimated from data. Finally, the last group describes uncertainties related to the extraction of the signal acceptance in MC simulation.

Source	Estimated uncertainty (%)	Treatment
e/ $\mu$ selection	3	flat
$\tau_h$ selection	5	flat
Trigger efficiency	1–3	flat
Jet energy scale	2–10	shape
b tag veto	1–2	shape
Pileup	1–5	shape
Integrated luminosity	2.6	flat
Scale variations and PDF (t $\bar{t}$ Z and t $\bar{t}$ W)	15	flat
Theoretical (ZZ)	25	flat
Conversions	15	flat
Other backgrounds	50	flat
Monte Carlo statistical precision	1–30	flat
Nonprompt leptons (closure)	30–36	flat
Nonprompt leptons (ewk subtraction)	5–20	shape
Charge misidentification	20	flat
WZ normalization	10	flat
WZ shape	5–50	shape
ISR uncertainty	1–5	shape
Scale variations for signal processes	1–2	shape
Lepton efficiencies	2	flat
Signal acceptance ( $E_T^{\text{miss}}$ modeling)	1–5	shape

The jet energy scale uncertainty varies between 2 and 10%, depending on the  $p_T$  and  $\eta$  of the jet. This uncertainty affects other event quantities such as the  $b$  tag veto,  $E_T^{\text{miss}}$ ,  $M_T$ , and  $M_{T2}$ , and is computed by shifting the energy of each jet coherently and propagating the variation to all these kinematic variables. Correlation effects due to the migration of events from one search region to another are taken into account. These variations yield estimated uncertainties ranging from 2 to 10% in the simulated signal and background yields in the different search regions. Similarly, the  $b$  jet veto efficiency is corrected for the differences between data and simulation, and an associated uncertainty in this correction is derived. The uncertainty in the modeling of pileup is 1–5%, depending on the search region, and the uncertainty in the integrated luminosity is 2.6% [60].

The uncertainty in the normalization of the  $WZ$  background is assessed to be 10%. This includes statistical uncertainties in the yields in the control sample used for normalization, and in the subtraction of the non- $WZ$  contributions to the sample. An additional uncertainty stems from the modeling of the  $M_T$  shape in the simulation of the  $WZ$  process. This uncertainty is found to be between 5 and 40%, from the comparison of the  $M_T$  shape in the  $WZ$  simulation with the one measured in the  $W\gamma$  control region. The size of this uncertainty increases for higher  $M_T$  values and is driven by the statistical uncertainty of the  $W\gamma$  control sample.

Further uncertainties in background yields estimated from simulations arise from the unknown higher-order effects in the theoretical calculations of the cross sections, and from uncertainties in the knowledge of the proton PDFs. The uncertainties from the proton PDFs are estimated by using the envelope of several PDF sets [61]. The effect of these theoretical uncertainties is found to be a 15% for  $t\bar{t}W$  and  $t\bar{t}Z$ , and 25% for  $ZZ$  backgrounds. Theoretical uncertainties are also considered for the remaining minor backgrounds estimated purely from simulation, in which 15% uncertainty is assigned to processes with a prompt  $\gamma$  modeled with NLO accuracy corresponding to the precision of the scale factor measured in the dedicated control region, and 50% to other rare processes.

Other sources of uncertainties are associated with the backgrounds, which are derived from, or normalized in, data control samples. The nonprompt background prediction has an uncertainty of 30% assigned to both light-lepton and  $\tau_h$  cases. This uncertainty arises from the performance of the method in the simulation in various regions of parameter space, and is given by the observed deviations between the estimated and observed yields in the control sample.

The uncertainty in the measurement of the charge misidentification background is derived from the difference between the yields of on- $Z$   $e^\pm e^\pm$  events in data and simulation. This uncertainty is found to be 20%.

Additional uncertainties in the signal acceptance extraction are considered for the ISR modeling, scale variation,  $E_T^{\text{miss}}$  modeling and lepton efficiencies due to the differences in simulations between signal and background samples.

## 8 Results

Some kinematic distributions are shown in Fig. 3 for the same-sign dilepton channel. Key kinematic distributions for the three-lepton channel are displayed in Fig. 5 and in Fig. 8 for three lepton events with at least one  $\tau_h$ . Fig. 10 displays the  $E_T^{\text{miss}}$  for events with four leptons.

The expected and observed yields are summarized in Table 11 for the same-sign channel, in Tables 12–17 for the trilepton channel and in Table 18 for the four-lepton channel. The observed event counts are consistent with those expected from the SM processes.

The comparisons between the expected and observed yields are presented in Fig. 4 for the same-sign dilepton channel, in Figs. 6-9 for the trilepton channel and in Fig. 11 for search regions with at least four leptons. Results for the aggregated search regions are presented in Fig. 12 and Table 19.

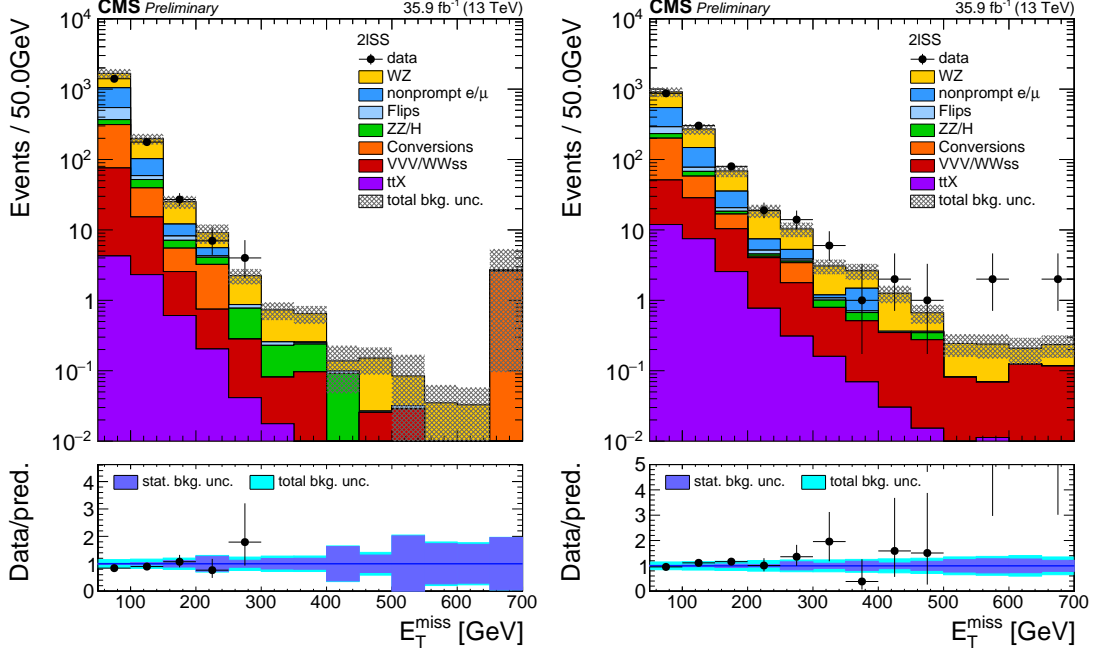


Figure 3: Distribution of the  $E_T^{\text{miss}}$  in events with 2 same-sign leptons and 0 jets (left) or 1 jet (right).

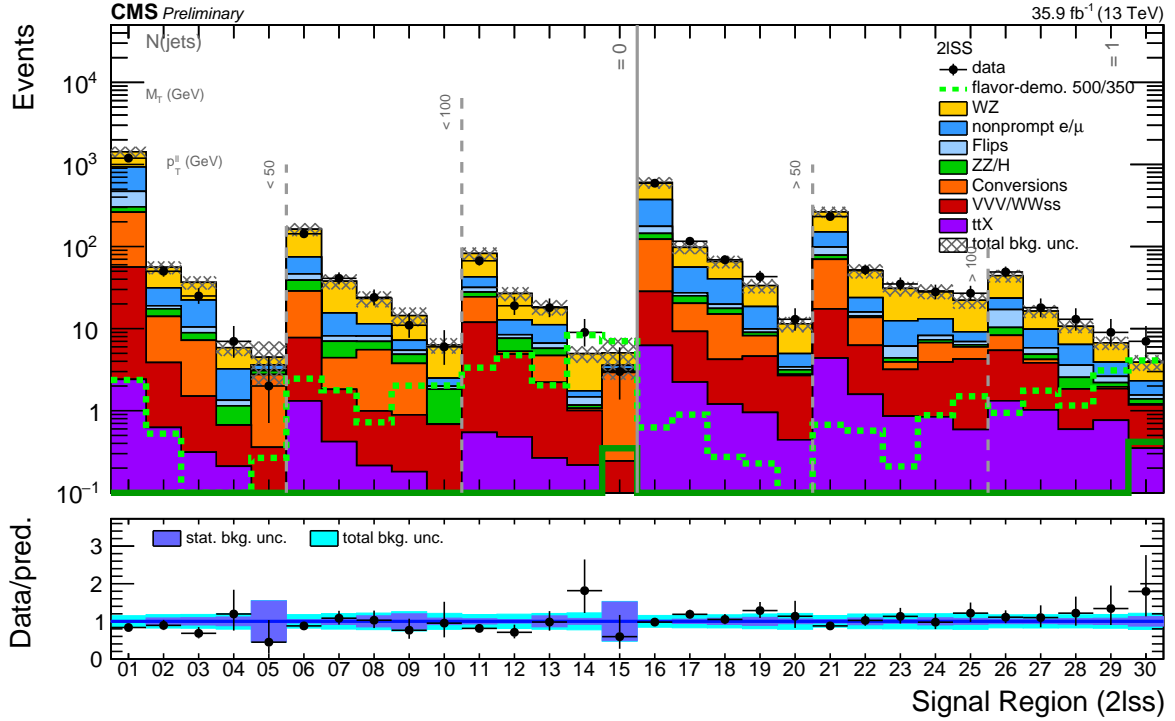


Figure 4: Expected and observed yields comparison in the same-sign category.

Table 11: Same-sign category: Expected and observed yields in events with two same-sign light leptons. The uncertainty denotes the total uncertainty on the result.

$N_{\text{jets}}$	$M_{\text{T}}$ (GeV)	$p_{\text{T}}^{\ell\ell}$ (GeV)	$E_{\text{T}}^{\text{miss}} < 100$ GeV	$100 \leq E_{\text{T}}^{\text{miss}} < 150$ GeV	$150 \leq E_{\text{T}}^{\text{miss}} < 200$ GeV	$E_{\text{T}}^{\text{miss}} \geq 200$ GeV
0	< 100	< 50	1426 $\pm$ 215	1193	$56 \pm 10$ 50 ++	6 $\pm$ 1 7 --
					$6 \pm 1$ 7 --	
		> 50	163 $\pm$ 29	143	$38 \pm 8$ 41 ++	14 $\pm$ 4 11
		> 100	82 $\pm$ 15	67	$23 \pm 5$ 24 --	
					$27 \pm 5$ 19 ++	5 $\pm$ 1 9
	1	< 100	603 $\pm$ 95	591	$66 \pm 11$ 69 --	33 $\pm$ 7 43
					$98 \pm 17$ 116 ++	
		> 50	264 $\pm$ 41	232	$51 \pm 10$ 52 ++	29 $\pm$ 6 28
					$31 \pm 6$ 35 --	
		> 100	44 $\pm$ 8	49	$16 \pm 3$ 18 ++	7 $\pm$ 1 9
		$11 \pm 2$ 13 --				
		3.9 $\pm$ 0.8 7				

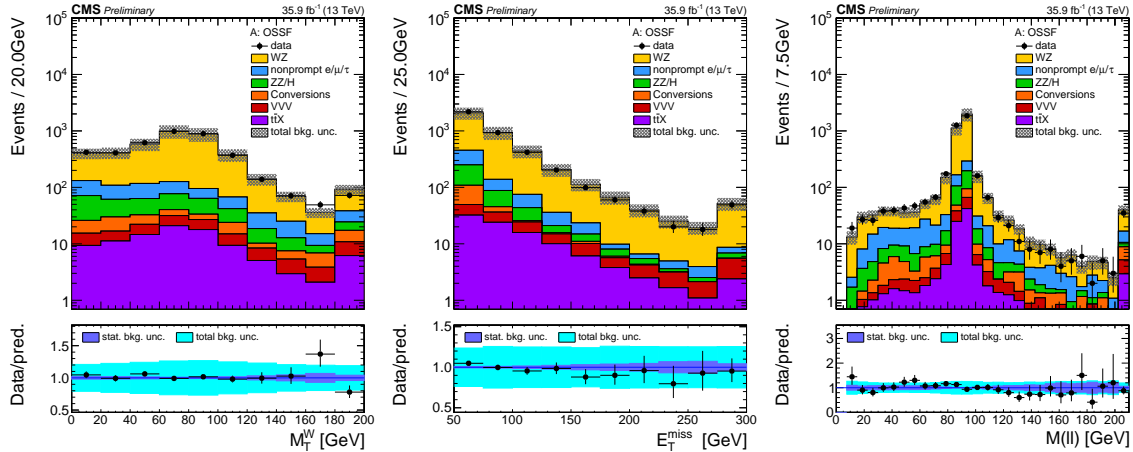


Figure 5: Distribution of key observables used in the event selection for events entering baseline region A: the transverse mass of the third lepton (left), the  $E_{\text{T}}^{\text{miss}}$  (middle) and the  $m_{\ell\ell\ell}$  (right) of the OSSF pair.

Table 12: Category A: Expected and observed yields in events with three e or  $\mu$  that form one OSSF pair. The uncertainty denotes the total uncertainty on the result.

$M_{\text{T}}$ (GeV)	$E_{\text{T}}^{\text{miss}}$ (GeV)	$M_{\ell\ell} < 75$ GeV	$75 \leq M_{\ell\ell} < 105$ GeV	$M_{\ell\ell} \geq 105$ GeV		
0 – 100	50 – 100	185 $\pm$ 36	186	2182 $\pm$ 550	2278	$121 \pm 25$ 123
	100 – 150	35 $\pm$ 8	34	441 $\pm$ 120	429	$32 \pm 7$ 32
	150 – 200	9 $\pm$ 2	11	129 $\pm$ 35	123	$12 \pm 3$ 4
	200 – 250	3 $\pm$ 1	1	48 $\pm$ 13	37	$2.9 \pm 0.8$ 6
	250 – 400	4 $\pm$ 1	5	42 $\pm$ 11	38	4 $\pm$ 1 5
	400 – 550			8 $\pm$ 2	5	
	$\geq 550$			2.6 $\pm$ 0.8	2	
100 – 160	50 – 100	50 $\pm$ 10	60	388 $\pm$ 101	391	$32 \pm 6$ 17
	100 – 150	15 $\pm$ 3	19	72 $\pm$ 18	61	$10 \pm 2$ 9
	150 – 200	1.9 $\pm$ 0.5	1	10 $\pm$ 2	9	$2.4 \pm 0.7$ 0
	$\geq 200$	0.8 $\pm$ 0.3	3	5 $\pm$ 1	8	$1.0 \pm 0.4$ 2
$\geq 160$	50 – 100	13 $\pm$ 3	16	37 $\pm$ 8	35	$9 \pm 2$ 9
	100 – 150	12 $\pm$ 3	17	21 $\pm$ 5	17	$7 \pm 1$ 3
	150 – 200	3.1 $\pm$ 1.0	4	9 $\pm$ 2	7	$3.1 \pm 0.9$ 0
	200 – 250	2.1 $\pm$ 0.6	3	4 $\pm$ 1	5	2.5 $\pm$ 0.6 0
	250 – 400	0.9 $\pm$ 0.3	1	4 $\pm$ 1	3	
	$\geq 400$			1.0 $\pm$ 0.3	1	

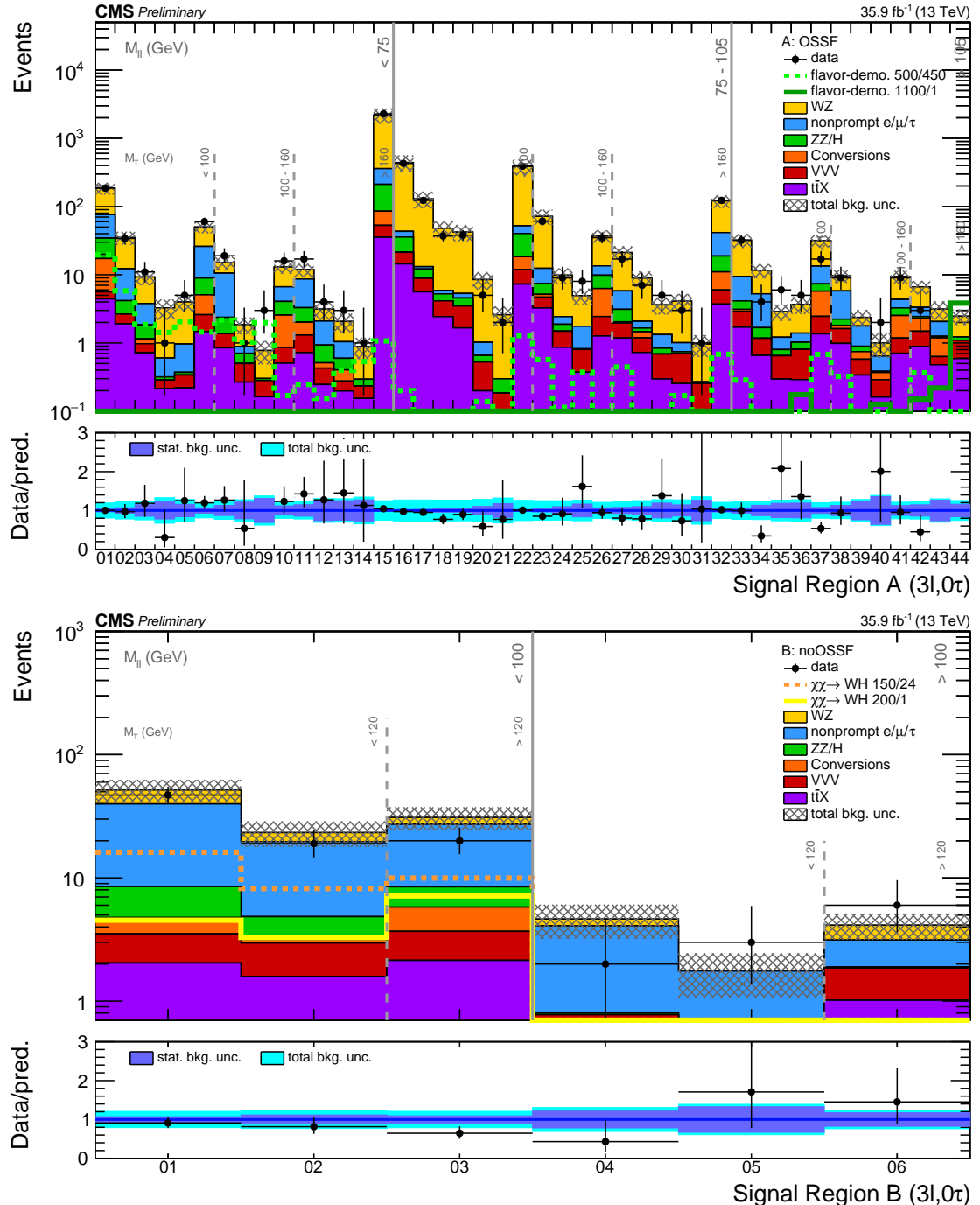


Figure 6: Expected and observed yields comparison in category A (top) and category B (bottom) signal regions, i.e. 3 light flavor leptons including at least one OSSF pair (A) or no OSSF pair (B), respectively.

Table 13: Category B: Expected and observed yields in events with three  $e$  or  $\mu$  that do not form an OSSF pair. The uncertainty denotes the total uncertainty on the result.

$M_T$ (GeV)	$E_T^{\text{miss}}$ (GeV)	$M_{\ell\ell} < 100$ GeV	$M_{\ell\ell} \geq 100$ GeV
0 – 120	50 – 100	$52 \pm 11$	47
	$\geq 100$	$23 \pm 5$	19
	$\geq 120$	$\geq 50$	$31 \pm 7$
		20	$4.1 \pm 1.0$
			6

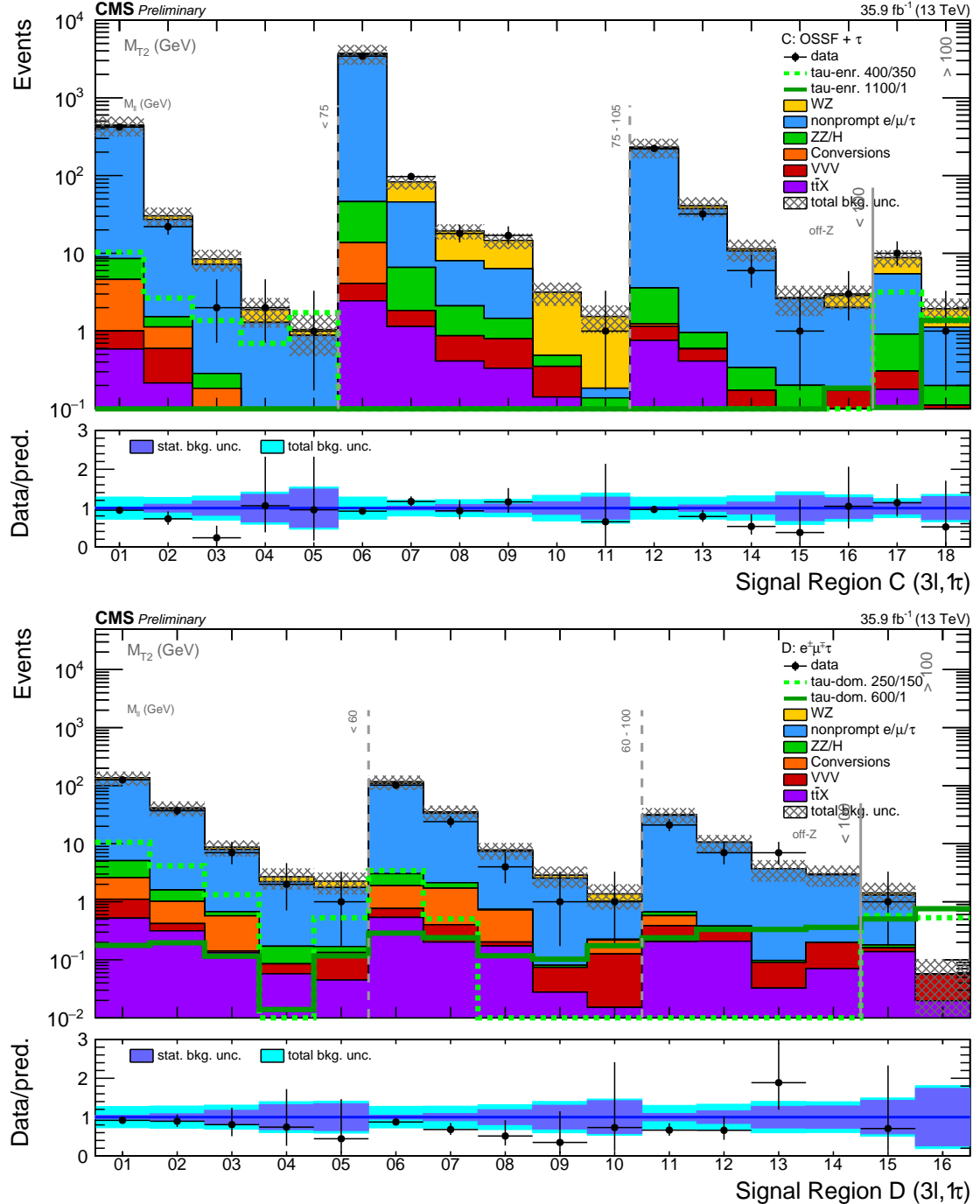


Figure 7: Expected and observed yields comparison in events with one  $\tau_h$ : categories C (top) and D (bottom).

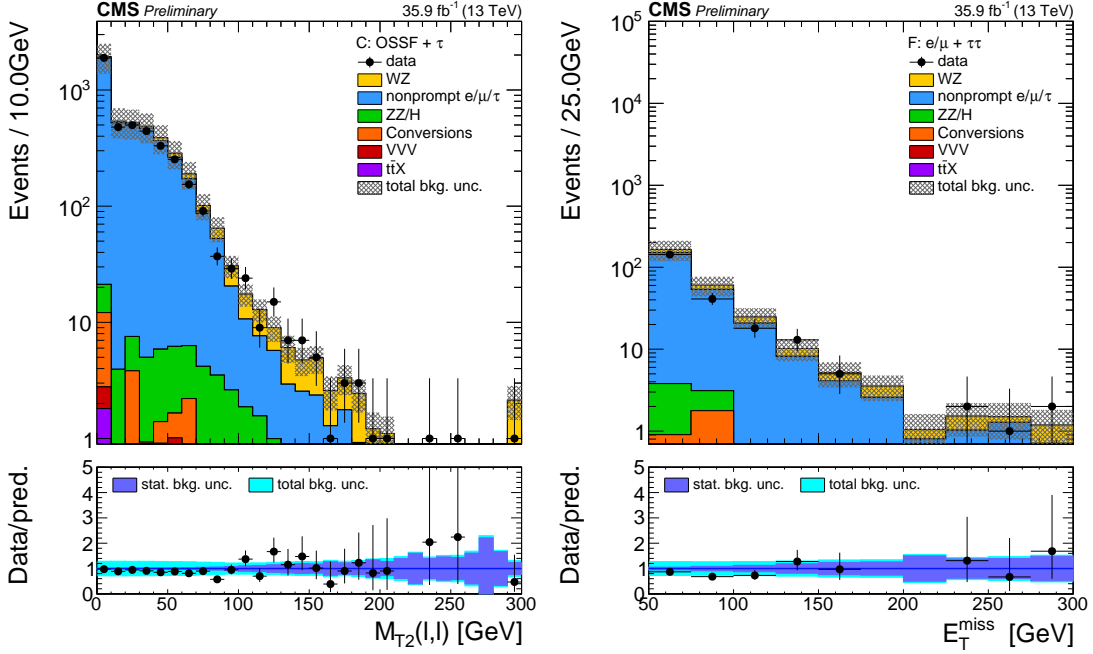


Figure 8: Distribution of the transverse mass in events with two OSSF light leptons and one hadronic tau (left) and  $E_T^{\text{miss}}$  in events with one light flavor lepton and two hadronic taus.

Table 14: Category C: Expected and observed yields in events with two e or  $\mu$  forming and OSSF pair and one  $\tau_h$ . The uncertainty denotes the total uncertainty on the result.

$E_T^{\text{miss}}$ (GeV)	$75 \leq M_{\ell\ell} < 105$ GeV	$M_{T2}(\ell_1, \ell_2)$ (GeV)	$M_{\ell\ell} < 75$ GeV	$M_{\ell\ell} \geq 105$ GeV
50 – 100	$3700 \pm 1100$	3427	0 – 100	$444 \pm 127$ 420
100 – 150	$83 \pm 17$	97		$30 \pm 8$ 22
150 – 200	$19 \pm 4$	18		$8 \pm 3$ 2
200 – 250	$15 \pm 3$	17		$1.9 \pm 0.8$ 2
250 – 300				$3 \pm 1$ 1
300 – 400	$3 \pm 1$	0		$2.9 \pm 1.0$ 3
$\geq 400$	$1.5 \pm 0.6$	1		$1.1 \pm 0.6$ 1
50 – 200			$\geq 100$	$9 \pm 2$ 10
$\geq 200$				$1.9 \pm 0.7$ 1

Table 15: Category D: Expected and observed yields in events with an opposite-sign e $\mu$  pair and one  $\tau_h$ . The uncertainty denotes the total uncertainty on the result.

$M_{T2}(\ell_1, \ell_2)$ (GeV)	$E_T^{\text{miss}}$ (GeV)	$M_{\ell\ell} < 60$ GeV	$60 \leq M_{\ell\ell} < 100$ GeV	$M_{\ell\ell} \geq 100$ GeV
0 – 100	50 – 100	$137 \pm 37$ 126	$117 \pm 32$ 102	$32 \pm 10$ 21
	100 – 150	$41 \pm 12$ 37	$35 \pm 10$ 24	$11 \pm 4$ 7
	150 – 200	$9 \pm 3$ 7	$8 \pm 2$ 4	$4 \pm 1$ 7
	200 – 250	$3 \pm 1$ 2	$3 \pm 1$ 1	$3 \pm 1$ 0
	$\geq 250$	$2.3 \pm 0.9$ 1	$1.4 \pm 0.6$ 1	
$\geq 100$	50 – 200	$1.4 \pm 0.7$		
	$\geq 200$	$0.06 \pm 0.04$		

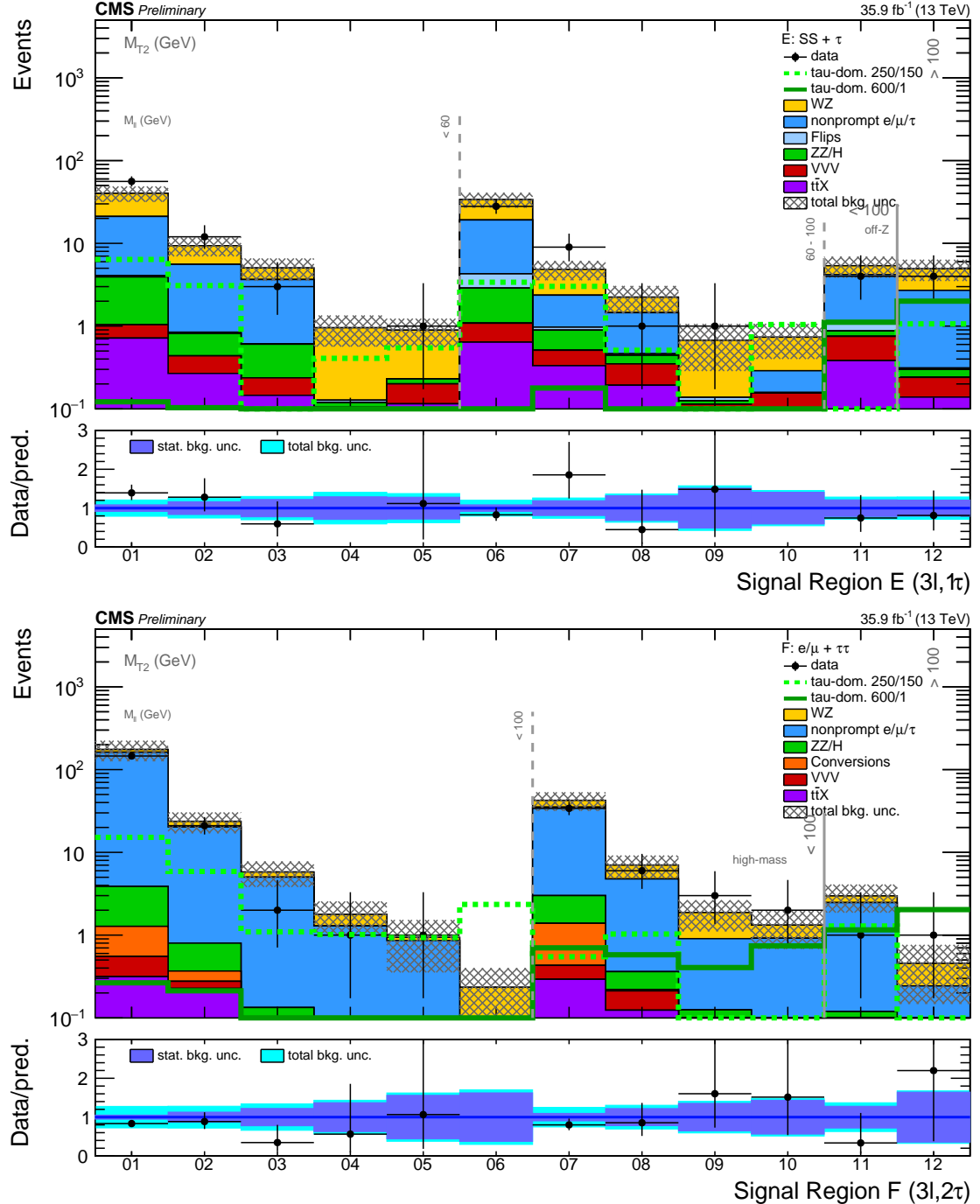


Figure 9: Expected and observed yields comparison in events one  $\tau_h$ : category E (top); and in events with two  $\tau_h$ : category F (bottom).

Table 16: Category E: Expected and observed yields in events with one same-sign  $e$  or  $\mu$  and one  $\tau_h$ . The uncertainty denotes the total uncertainty on the result.

Table 17: Category F: Expected and observed yields in events with one  $e$  or  $\mu$  and two  $\tau_h$ . The uncertainty denotes total uncertainty on the result.

$M_{\mathrm{T2}}(\ell, \tau_1)$ (GeV)	$E_{\mathrm{T}}^{\mathrm{miss}}$ (GeV)	$M_{\ell\ell} < 100$ GeV	$M_{\ell\ell} \geq 100$ GeV
0 – 100	50 – 100	$175 \pm 49$	146
	100 – 150	$24 \pm 7$	21
	150 – 200	$6 \pm 2$	2
	200 – 250	$1.8 \pm 0.8$	1
	250 – 300	$0.9 \pm 0.6$	1
	$\geq 300$	$0.2 \pm 0.2$	0
$\geq 100$	50 – 200	$3 \pm 1$	1
	$\geq 200$	$0.5 \pm 0.3$	1

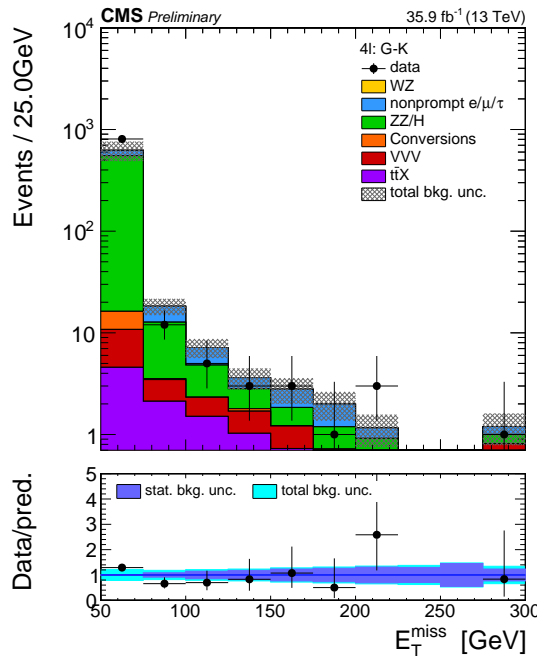


Figure 10: Distribution of the  $E_T^{\text{miss}}$  in events with 4 or more leptons entering search categories G-K.

Table 18: Categories G-K: Expected and observed yields in the  $4\ell$  category of the analysis. The uncertainty denotes the total uncertainty on the result.

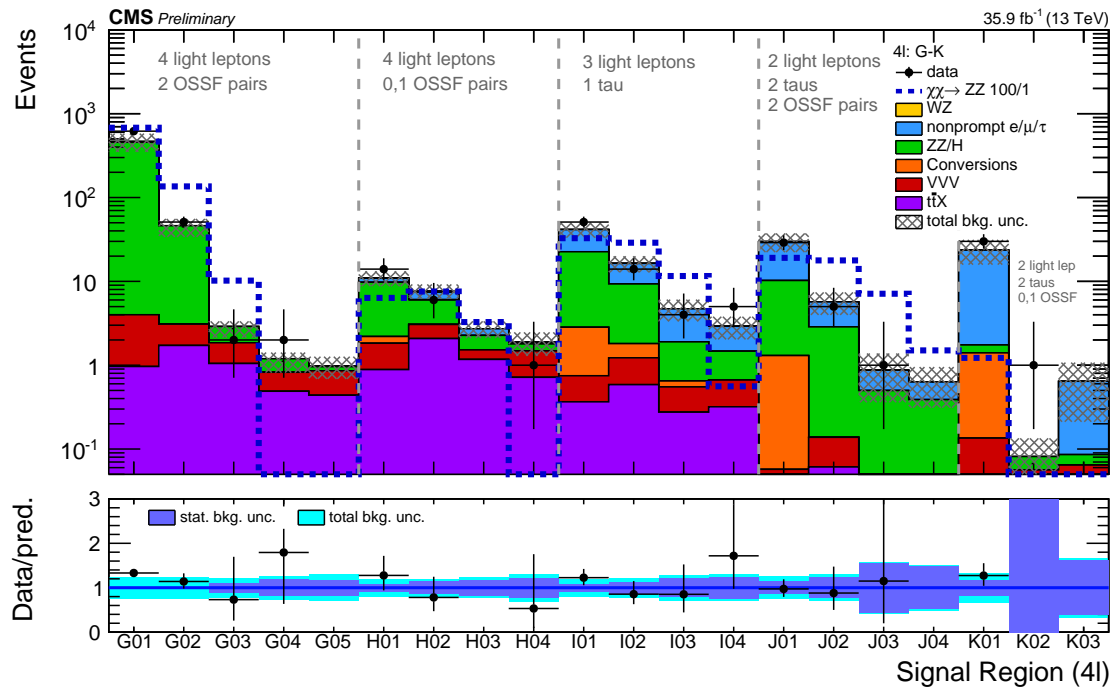


Figure 11: Expected and observed yields comparison in signal regions with at least four leptons (categories G-K).

Table 19: Expected and observed yields in the aggregated signal defined in Section 5.3. The uncertainty denotes the total uncertainty on the result.

nb	final state	definition	event yield	
1	2 same-sign leptons	$0 \text{ jets, } M_T > 100 \text{ GeV and } E_T^{\text{miss}} > 140 \text{ GeV}$	$12 \pm 3$	13
2	2 same-sign leptons	$1 \text{ jets, } M_T < 100 \text{ GeV, } p_T^{\ell\ell} < 100 \text{ GeV and } E_T^{\text{miss}} > 200 \text{ GeV}$	$18 \pm 4$	18
3	3 light leptons	$M_T > 120 \text{ GeV and } E_T^{\text{miss}} > 200 \text{ GeV}$	$19 \pm 4$	19
4	3 light leptons	$E_T^{\text{miss}} > 250 \text{ GeV}$	$142 \pm 34$	128
5	2 light leptons and 1 tau	$M_{T2}(\ell_1, \tau) > 50 \text{ GeV and } E_T^{\text{miss}} > 200 \text{ GeV}$	$22 \pm 5$	18
6	1 light lepton and 2 taus	$M_{T2}(\ell, \tau_1) > 50 \text{ GeV and } E_T^{\text{miss}} > 200 \text{ GeV}$	$1.2 \pm 0.6$	2
7	1 light lepton and 2 taus	$E_T^{\text{miss}} > 75 \text{ GeV}$	$109 \pm 28$	82
8	more than 3 leptons	$E_T^{\text{miss}} > 200 \text{ GeV}$	$197 \pm 42$	166

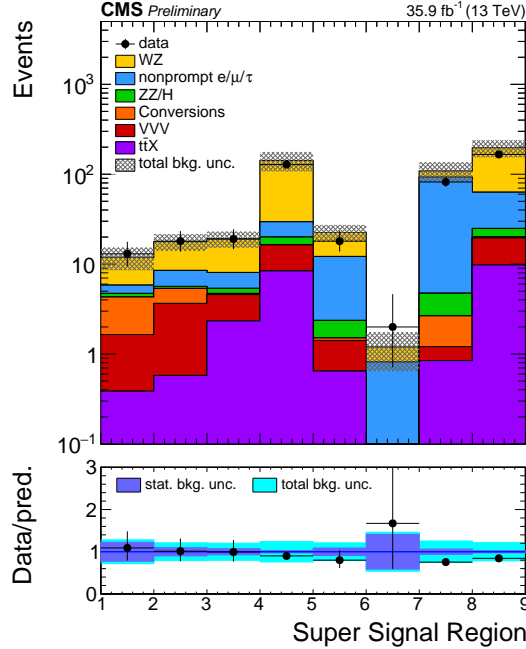


Figure 12: Expected and observed yields comparison in the aggregated search regions. In this plot, the data-driven charge flip prediction (that is only relevant in the first two bins due to the same-sign dilepton final state) are included in the data-driven nonprompt background prediction.

## 9 Interpretations of the searches

Having found no evidence of any significant deviation with respect to the SM prediction, the results of this search are interpreted in the context of the simplified models covering the scenarios described in Section 2.

We compute 95% confidence level (CL) upper limits on the new-physics cross sections using the  $CL_s$  method [62–64], incorporating the uncertainties on the signal efficiency and acceptance and the uncertainties on the expected background described in Section 7. Lognormal nuisance parameters are used for the signal and background estimate uncertainties. The NLO+NLL (next-to-leading logarithmic accuracy) cross sections from Refs. [65–67] are used to derive constraints on the masses of the charginos and neutralinos. Only the categories with the lepton flavor, multiplicity and charge requirements corresponding to the topology of the interpreted model are combined in order to increase sensitivity to the model in question.

The interpretation of the results are displayed in Figures 13–17 for all the models described in Section 2. Every plot shows the 95% CL upper limit on the chargino-neutralino production cross section times branching fraction. The observed,  $\pm 1\sigma_{\text{theory}}$  observed, median expected, and  $\pm 1\sigma_{\text{experiment}}$  expected contours are also shown. Table 20 summarizes which search regions have been used for the interpretation of the results for each model. The figure displaying each interpretation is also mentioned in the table.

Table 20: Summary of the interpretations of the results using different models .

Model	Categories Used	Figure
$\tilde{\chi}_1^\pm \tilde{\chi}_2^0$ production, flavor-democratic, $m_{\tilde{\ell}} = m_{\tilde{\chi}_1^0} + 0.5 \cdot (m_{\tilde{\chi}_2^0} - m_{\tilde{\chi}_1^0})$	A	13
$\tilde{\chi}_1^\pm \tilde{\chi}_2^0$ production, flavor-democratic, $m_{\tilde{\ell}} = m_{\tilde{\chi}_1^0} + 0.05 \cdot (m_{\tilde{\chi}_2^0} - m_{\tilde{\chi}_1^0})$	SS, A	14 (left)
$\tilde{\chi}_1^\pm \tilde{\chi}_2^0$ production, flavor-democratic, $m_{\tilde{\ell}} = m_{\tilde{\chi}_1^0} + 0.95 \cdot (m_{\tilde{\chi}_2^0} - m_{\tilde{\chi}_1^0})$	SS, A	14 (right)
$\tilde{\chi}_1^\pm \tilde{\chi}_2^0$ production, $\tau$ -enriched, $m_{\tilde{\ell}} = m_{\tilde{\chi}_1^0} + 0.05 \cdot (m_{\tilde{\chi}_2^0} - m_{\tilde{\chi}_1^0})$	A, C	15 (left)
$\tilde{\chi}_1^\pm \tilde{\chi}_2^0$ production, $\tau$ -enriched, $m_{\tilde{\ell}} = m_{\tilde{\chi}_1^0} + 0.5 \cdot (m_{\tilde{\chi}_2^0} - m_{\tilde{\chi}_1^0})$	A, C	15 (center)
$\tilde{\chi}_1^\pm \tilde{\chi}_2^0$ production, $\tau$ -enriched, $m_{\tilde{\ell}} = m_{\tilde{\chi}_1^0} + 0.95 \cdot (m_{\tilde{\chi}_2^0} - m_{\tilde{\chi}_1^0})$	A, C	15 (right)
$\tilde{\chi}_1^\pm \tilde{\chi}_2^0$ production, $\tau$ -dominated, $m_{\tilde{\tau}} = m_{\tilde{\chi}_1^0} + 0.5 \cdot (m_{\tilde{\chi}_2^0} - m_{\tilde{\chi}_1^0})$	B-F	16
$\tilde{\chi}_1^\pm \tilde{\chi}_2^0$ production, heavy sleptons, $\tilde{\chi}_1^\pm \tilde{\chi}_2^0 \rightarrow WZ$	A	17 (left)
$\tilde{\chi}_1^\pm \tilde{\chi}_2^0$ production, heavy sleptons, $\tilde{\chi}_1^\pm \tilde{\chi}_2^0 \rightarrow WH$	SS, A-K	17 (right)

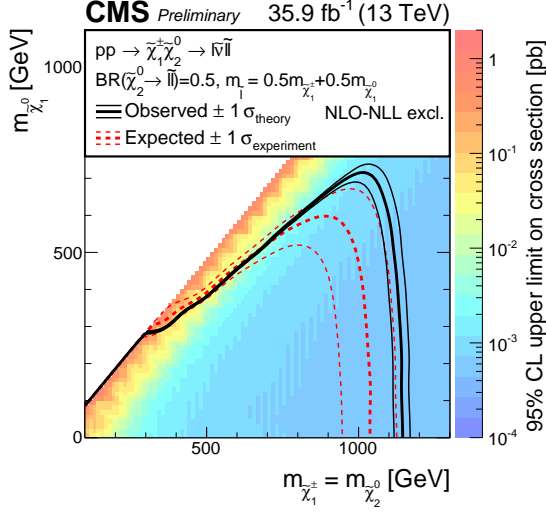


Figure 13: Interpretation of the results in the flavor-democratic model with mass parameter  $x = 0.5$  obtained with events of category A. The shading in the  $m_{\tilde{\chi}_1^0}$  versus  $m_{\tilde{\chi}_2^0}$  ( $= m_{\tilde{\chi}_1^\pm}$ ) plane indicates the 95% CL upper limit on the chargino-neutralino production cross section times branching fraction. The contours bound the mass regions excluded at 95% CL assuming the NLO+NLL cross sections. The observed,  $\pm 1\sigma_{\text{theory}}$  observed, median expected, and  $\pm 1\sigma_{\text{experiment}}$  expected bounds are shown.

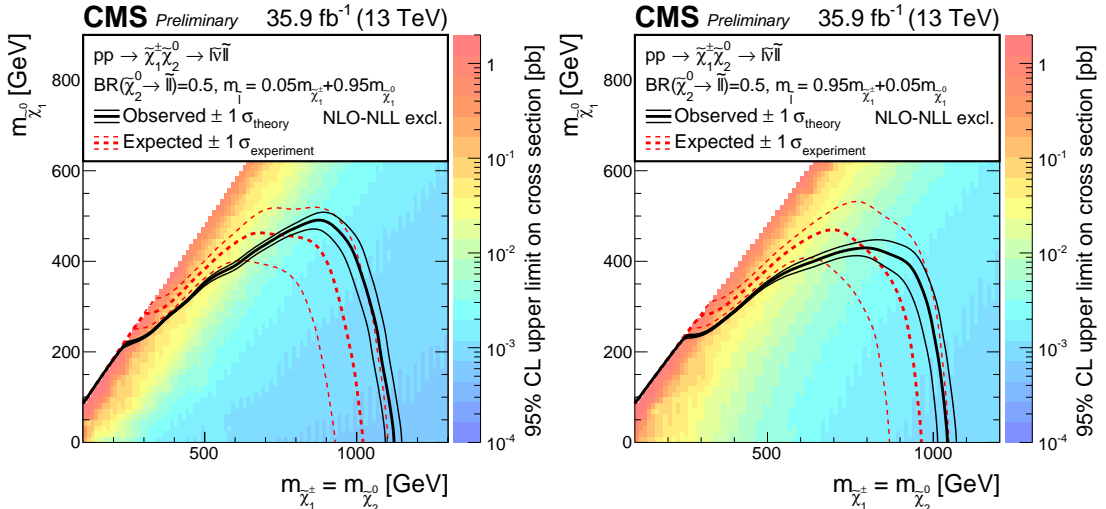


Figure 14: Interpretation of the results in the flavor-democratic model with mass parameter  $x = 0.05$  (left) and  $x = 0.95$  (right) obtained with the combination of the same-sign category and category A. The shading in this figure are as described in Figure 13.

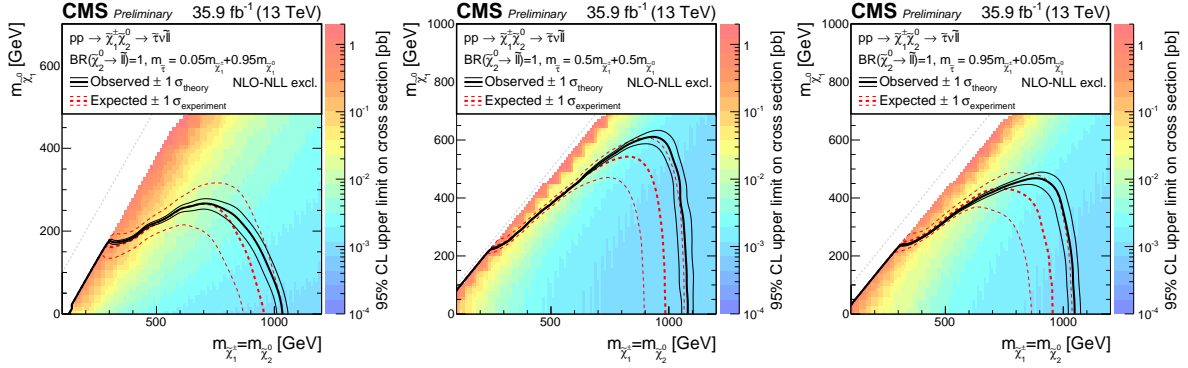


Figure 15: Interpretation of the results in the tau-enriched model with mass parameter  $x = 0.05$  (left),  $x = 0.5$  (center) and  $x = 0.95$  (right) obtained with events of categories A and C. The shading in this figure are as described in Figure 13.

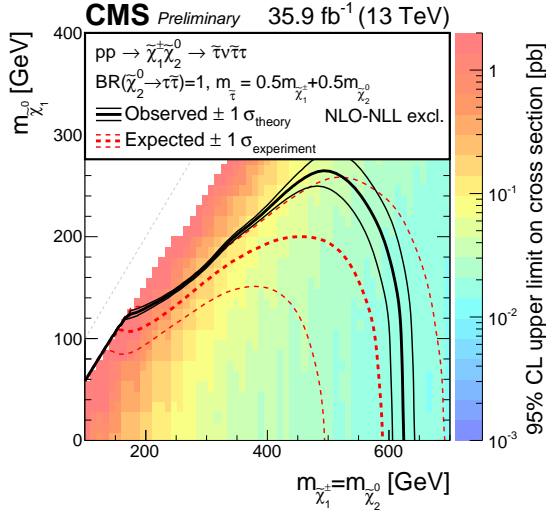


Figure 16: Interpretation of the results in the tau-dominated model with mass parameter  $x = 0.5$  obtained with events of category B-F. The shading in this figure are as described in Figure 13.

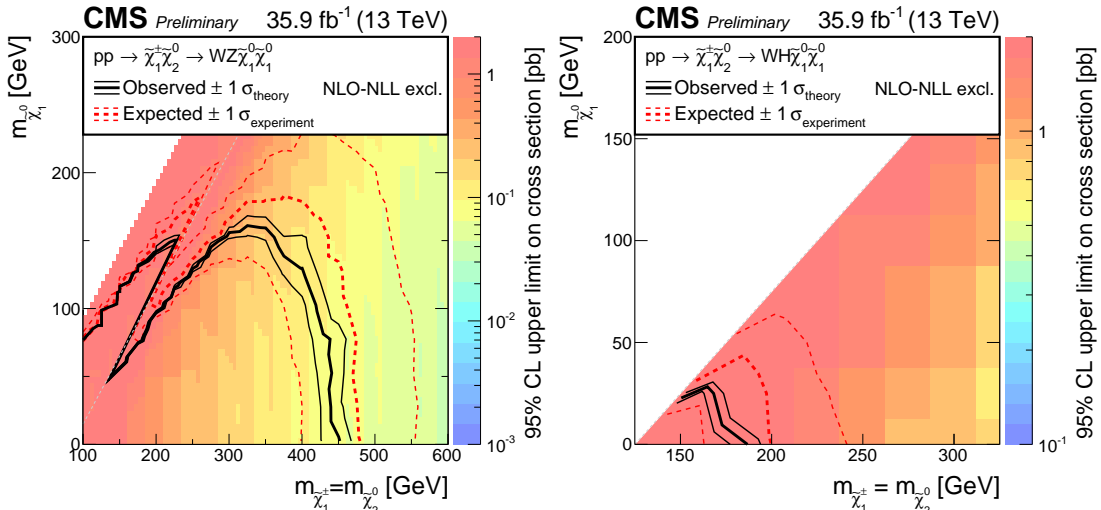


Figure 17: Interpretation of the results in the  $\tilde{\chi}_1^\pm \tilde{\chi}_2^0 \rightarrow WZ \tilde{\chi}_1^0$  (left) model obtained with events of category A and the  $\tilde{\chi}_1^\pm \tilde{\chi}_2^0 \rightarrow WH \tilde{\chi}_1^0$  (right) model obtained with events of all categories (same-sign, trilepton and four lepton). The shading in this figure are as described in Figure 13.

## 10 Summary

Results are presented of a search for new physics in same-sign dilepton, trilepton, and four-lepton events containing up to two hadronically decaying  $\tau$  leptons in  $pp$  collision data at  $\sqrt{s} = 13$  TeV, recorded with the CMS detector at the LHC and corresponding to an integrated luminosity of  $35.9 \text{ fb}^{-1}$ . The data are divided into categories based on the number, charge, and flavor of the leptons, and subdivided into various kinematic regions to be sensitive to a broad range of electroweakly produced new particles.

No significant deviation from the standard model expectations is observed. The results are used to set limits on various simplified models of supersymmetry that entail the production of superpartners of gauge or Higgs bosons (charginos and neutralinos). Specifically we consider chargino-neutralino pair production, an electroweak process that is expected to have the largest cross section. The resulting signal topologies depend on the masses of the lepton superpartners (sleptons). Models with light left-handed sleptons lead to enhanced branching fractions to final states with three leptons. Depending on the left-right mixing and flavor of these sleptons, the results imply limits on the masses of charginos and neutralinos up to 1150 GeV for the flavor-democratic scenario, extending the reach of our previous result [15] by about 450 GeV. In these models, searches in the same-sign dilepton final state enhance the sensitivity in the experimentally challenging region with small mass difference between the produced gauginos and the lightest supersymmetric particle that are inaccessible with the trilepton signature.

In the case in which the chargino and neutralino decay ultimately to three  $\tau$  leptons and the lightest supersymmetric particle, masses of charginos up to 400 GeV are probed.

The most challenging scenarios considered involve the direct decay of gauginos to the lightest supersymmetric particle via W and Z or Higgs bosons. For the final states with W and Z bosons, chargino masses up to 475 GeV are excluded, improving the previous reach by 200 GeV. In the case of neutralino decay via a Higgs boson, only masses up to 225 GeV can be excluded.

## References

- [1] ATLAS Collaboration, “Observation of a new particle in the search for the Standard Model Higgs boson with the ATLAS detector at the LHC”, *Phys. Lett. B* **716** (2012) 1, doi:10.1016/j.physletb.2012.08.020, arXiv:1207.7214.
- [2] CMS Collaboration, “Observation of a new boson at a mass of 125 GeV with the CMS experiment at the LHC”, *Phys. Lett. B* **716** (2012) 30, doi:10.1016/j.physletb.2012.08.021, arXiv:1207.7235.
- [3] CMS Collaboration, “Observation of a new boson with mass near 125 GeV in pp collisions at  $\sqrt{s} = 7$  and 8 TeV”, *JHEP* **06** (2013) 081, doi:10.1007/JHEP06(2013)081, arXiv:1303.4571.
- [4] P. Ramond, “Dual theory for free fermions”, *Phys. Rev. D* **3** (1971) 2415, doi:10.1103/PhysRevD.3.2415.
- [5] Yu. A. Golfand and E. P. Likhtman, “Extension of the algebra of Poincare group generators and violation of P invariance”, *JETP Lett.* **13** (1971) 323. [Pisma Zh. Eksp. Teor. Fiz. **13** (1971) 452].
- [6] A. Neveu and J. H. Schwarz, “Factorizable dual model of pions”, *Nucl. Phys. B* **31** (1971) 86, doi:10.1016/0550-3213(71)90448-2.
- [7] D. V. Volkov and V. P. Akulov, “Possible universal neutrino interaction”, *JETP Lett.* **16** (1972) 438. [Pisma Zh. Eksp. Teor. Fiz. **16** (1972) 621].
- [8] J. Wess and B. Zumino, “A lagrangian model invariant under supergauge transformations”, *Phys. Lett. B* **49** (1974) 52, doi:10.1016/0370-2693(74)90578-4.
- [9] J. Wess and B. Zumino, “Supergauge transformations in four-dimensions”, *Nucl. Phys. B* **70** (1974) 39, doi:10.1016/0550-3213(74)90355-1.
- [10] P. Fayet, “Supergauge invariant extension of the Higgs mechanism and a model for the electron and its neutrino”, *Nucl. Phys. B* **90** (1975) 104, doi:10.1016/0550-3213(75)90636-7.
- [11] H. P. Nilles, “Supersymmetry, supergravity and particle physics”, *Phys. Rept.* **110** (1984) 1, doi:10.1016/0370-1573(84)90008-5.
- [12] S. P. Martin, “A supersymmetry primer”, in *Perspectives on Supersymmetry II*, G. L. Kane, ed., p. 1. 2010. arXiv:hep-ph/9709356. Adv. Ser. Direct. High Energy Phys., vol. 21. doi:10.1142/9789814307505\_0001.
- [13] ATLAS Collaboration, “Summary of the ATLAS experiment’s sensitivity to supersymmetry after LHC Run 1 – interpreted in the phenomenological MSSM”, *JHEP* **10** (2015) 134, doi:10.1007/JHEP10(2015)134, arXiv:1508.06608.
- [14] CMS Collaboration, “Phenomenological MSSM interpretation of CMS searches in pp collisions at  $\sqrt{s} = 7$  and 8 TeV”, *JHEP* **10** (2016) 129, doi:10.1007/JHEP10(2016)129, arXiv:1606.03577.
- [15] CMS Collaboration, “Searches for electroweak production of charginos, neutralinos, and sleptons decaying to leptons and W, Z, and Higgs bosons in pp collisions at 8 TeV”, *Eur. Phys. J. C* **74** (2014) 3036, doi:10.1140/epjc/s10052-014-3036-7, arXiv:1405.7570.

- [16] CMS Collaboration, “Searches for electroweak neutralino and chargino production in channels with Higgs, Z, and W bosons in pp collisions at 8 TeV”, *Phys. Rev. D* **90** (2014) 092007, doi:10.1103/PhysRevD.90.092007, arXiv:1409.3168.
- [17] ATLAS Collaboration, “Search for the electroweak production of supersymmetric particles in  $\sqrt{s}=8$  TeV pp collisions with the ATLAS detector”, *Phys. Rev. D* **93** (2016) 052002, doi:10.1103/PhysRevD.93.052002, arXiv:1509.07152.
- [18] CMS Collaboration, “Search for supersymmetry in the multijet and missing transverse momentum final state in pp collisions at 13 TeV”, *Phys. Lett. B* **758** (2016) 152, doi:10.1016/j.physletb.2016.05.002, arXiv:1602.06581.
- [19] CMS Collaboration, “Search for new physics with the  $M_{T2}$  variable in all-jets final states produced in pp collisions at  $\sqrt{s} = 13$  TeV”, *JHEP* **10** (2016) 006, doi:10.1007/JHEP10(2016)006, arXiv:1603.04053.
- [20] CMS Collaboration, “Search for supersymmetry in pp collisions at  $\sqrt{s} = 13$  TeV in the single-lepton final state using the sum of masses of large-radius jets”, *JHEP* **08** (2016) 122, doi:10.1007/JHEP08(2016)122, arXiv:1605.04608.
- [21] CMS Collaboration, “Search for new physics in same-sign dilepton events in proton-proton collisions at  $\sqrt{s} = 13$  TeV”, *Eur. Phys. J. C* **76** (2016) 439, doi:10.1140/epjc/s10052-016-4261-z, arXiv:1605.03171.
- [22] ATLAS Collaboration, “Search for squarks and gluinos in final states with jets and missing transverse momentum at  $\sqrt{s} = 13$  TeV with the ATLAS detector”, *Eur. Phys. J. C* **76** (2016) 392, doi:10.1140/epjc/s10052-016-4184-8, arXiv:1605.03814.
- [23] ATLAS Collaboration, “Search for gluinos in events with an isolated lepton, jets and missing transverse momentum at  $\sqrt{s} = 13$  TeV with the ATLAS detector”, *Eur. Phys. J. C* **76** (2016) 565, doi:10.1140/epjc/s10052-016-4397-x, arXiv:1605.04285.
- [24] ATLAS Collaboration, “Search for pair production of gluinos decaying via stop and sbottom in events with b-jets and large missing transverse momentum in pp collisions at  $\sqrt{s} = 13$  TeV with the ATLAS detector”, *Phys. Rev. D* **94** (2016), no. 3, 032003, doi:10.1103/PhysRevD.94.032003, arXiv:1605.09318.
- [25] CMS Collaboration, “Search for electroweak SUSY production in multilepton final states in pp collisions at  $\sqrt(s) = 13$  TeV with 12.9/fb”, CMS Physics Analysis Summary CMS-PAS-SUS-16-024, CERN, 2016.
- [26] ATLAS Collaboration, “Search for supersymmetry with two and three leptons and missing transverse momentum in the final state at  $\sqrt{s} = 13$  TeV with the ATLAS detector”, ATLAS Conference Note ATLAS-CONF-2016-096, CERN, 2016.
- [27] D. Alves et al., “Simplified models for LHC new physics searches”, *J. Phys. G* **39** (2012) 105005, doi:10.1088/0954-3899/39/10/105005, arXiv:1105.2838.
- [28] CMS Collaboration, “The CMS experiment at the CERN LHC”, *JINST* **3** (2008) S08004, doi:10.1088/1748-0221/3/08/S08004.
- [29] CMS Collaboration, “Particle-Flow Event Reconstruction in CMS and Performance for Jets, Taus, and MET”, CMS Physics Analysis Summary CMS-PAS-PFT-09-001, CERN, 2009.

[30] CMS Collaboration, “Commissioning of the Particle–Flow reconstruction in Minimum–Bias and Jet Events from pp Collisions at 7 TeV”, CMS Physics Analysis Summary CMS-PAS-PFT-10-002, CERN, 2010.

[31] CMS Collaboration, “Performance of electron reconstruction and selection with the CMS detector in proton–proton collisions at  $\sqrt{s} = 8$  TeV”, *JINST* **10** (2015) P06005, doi:10.1088/1748-0221/10/06/P06005, arXiv:1502.02701.

[32] CMS Collaboration, “Performance of CMS muon reconstruction in pp collision events at  $\sqrt{s} = 7$  TeV”, *JINST* **7** (2012) P10002, doi:10.1088/1748-0221/7/10/P10002, arXiv:1206.4071.

[33] K. Rehermann and B. Tweedie, “Efficient identification of boosted semileptonic top quarks at the LHC”, *JHEP* **03** (2011) 059, doi:10.1007/JHEP03(2011)059, arXiv:1007.2221.

[34] CMS Collaboration, “Search for new physics in same-sign dilepton events in proton–proton collisions at  $\sqrt{s} = 13$  TeV”, *Eur. Phys. J.* **C76** (2016), no. 8, 439, doi:10.1140/epjc/s10052-016-4261-z, arXiv:1605.03171.

[35] B. P. Roe et al., “Boosted decision trees, an alternative to artificial neural networks”, *Nucl. Instrum. Meth. A* **543** (2005) 577, doi:10.1016/j.nima.2004.12.018, arXiv:physics/0408124.

[36] CMS Collaboration, “Search for  $t\bar{t}H$  production in multilepton final states at  $\sqrt{s} = 13$  TeV”, CMS Physics Analysis Summary CMS-PAS-HIG-15-008, 2016.

[37] CMS Collaboration, “Reconstruction and identification of  $\tau$  lepton decays to hadrons and  $\nu_\tau$  at CMS”, *JINST* **11** (2016) P01019, doi:10.1088/1748-0221/11/01/P01019, arXiv:1510.07488.

[38] CMS Collaboration, “Performance of reconstruction and identification of tau leptons in their decays to hadrons and tau neutrino in LHC Run-2”, CMS Physics Analysis Summary CMS-PAS-TAU-16-002, CERN, 2016.

[39] M. Cacciari, G. P. Salam, and G. Soyez, “The anti- $k_t$  jet clustering algorithm”, *JHEP* **04** (2008) 063, doi:10.1088/1126-6708/2008/04/063, arXiv:0802.1189.

[40] M. Cacciari, G. P. Salam, and G. Soyez, “FastJet User Manual”, *Eur. Phys. J. C* **72** (2012) 1896, doi:10.1140/epjc/s10052-012-1896-2, arXiv:1111.6097.

[41] M. Cacciari and G. P. Salam, “Dispelling the  $N^3$  myth for the  $k_t$  jet-finder”, *Phys. Lett. B* **641** (2006) 57, doi:10.1016/j.physletb.2006.08.037, arXiv:hep-ph/0512210.

[42] CMS Collaboration, “Determination of jet energy calibration and transverse momentum resolution in CMS”, *JINST* **6** (2011) P11002, doi:10.1088/1748-0221/6/11/P11002, arXiv:1107.4277.

[43] M. Cacciari and G. P. Salam, “Pileup subtraction using jet areas”, *Phys. Lett. B* **659** (2008) 119–126, doi:10.1016/j.physletb.2007.09.077, arXiv:0707.1378.

[44] CMS Collaboration, “Study of Pileup Removal Algorithms for Jets”, CMS Physics Analysis Summary CMS-PAS-JME-14-001, CERN, 2014.

- [45] CMS Collaboration, “Jet energy scale and resolution in the CMS experiment in pp collisions at 8 TeV”, *JINST* **12** (2017), no. 02, P02014, doi:10.1088/1748-0221/12/02/P02014, arXiv:1607.03663.
- [46] CMS Collaboration, “Identification of b quark jets at the CMS Experiment in the LHC Run 2”, CMS Physics Analysis Summary CMS-PAS-BTV-15-001, CERN, 2016.
- [47] CMS Collaboration, “Identification of b-quark jets with the CMS experiment”, *JINST* **8** (2013) P04013, doi:10.1088/1748-0221/8/04/P04013, arXiv:1211.4462.
- [48] CMS Collaboration, “Performance of the CMS missing transverse momentum reconstruction in pp data at  $\sqrt{s} = 8$  TeV”, *JINST* **10** (2015) P02006, doi:10.1088/1748-0221/10/02/P02006, arXiv:1411.0511.
- [49] J. Alwall et al., “The automated computation of tree-level and next-to-leading order differential cross sections, and their matching to parton shower simulations”, *JHEP* **07** (2014) 079, doi:10.1007/JHEP07(2014)079, arXiv:1405.0301.
- [50] T. Melia, P. Nason, R. Rontsch, and G. Zanderighi, “ $W^+W^-$ ,  $WZ$  and  $ZZ$  production in the POWHEG BOX”, *JHEP* **11** (2011) 078, doi:10.1007/JHEP11(2011)078, arXiv:1107.5051.
- [51] P. Nason and G. Zanderighi, “ $W^+W^-$ ,  $WZ$  and  $ZZ$  production in the POWHEG-BOX-V2”, *Eur. Phys. J. C* **74** (2014) 2702, doi:10.1140/epjc/s10052-013-2702-5, arXiv:1311.1365.
- [52] NNPDF Collaboration, “Parton distributions for the LHC Run II”, *JHEP* **04** (2015) 040, doi:10.1007/JHEP04(2015)040, arXiv:1410.8849.
- [53] T. Sjöstrand, S. Mrenna, and P. Z. Skands, “A brief introduction to PYTHIA 8.1”, *Comput. Phys. Commun.* **178** (2008) 852, doi:10.1016/j.cpc.2008.01.036, arXiv:0710.3820.
- [54] P. Skands, S. Carrazza, and J. Rojo, “Tuning PYTHIA 8.1: the Monash 2013 tune”, *Eur. Phys. J. C* **74** (2014) 3024, doi:10.1140/epjc/s10052-014-3024-y, arXiv:1404.5630.
- [55] CMS Collaboration, “Event generator tunes obtained from underlying event and multiparton scattering measurements”, *Eur. Phys. J. C* **76** (2016) 155, doi:10.1140/epjc/s10052-016-3988-x, arXiv:1512.00815.
- [56] GEANT4 Collaboration, “GEANT4—a simulation toolkit”, *Nucl. Instrum. Meth. A* **506** (2003) 250, doi:10.1016/S0168-9002(03)01368-8.
- [57] S. Abdullin et al., “The fast simulation of the CMS detector at LHC”, *J. Phys. Conf. Ser.* **331** (2011) 032049, doi:10.1088/1742-6596/331/3/032049.
- [58] C. G. Lester and D. J. Summers, “Measuring masses of semiinvisibly decaying particles pair produced at hadron colliders”, *Phys. Lett. B* **463** (1999) 99, doi:10.1016/S0370-2693(99)00945-4, arXiv:hep-ph/9906349.
- [59] A. Barr, C. Lester, and P. Stephens, “m(T2): The truth behind the glamour”, *J. Phys. G* **29** (2003) 2343, doi:10.1088/0954-3899/29/10/304, arXiv:hep-ph/0304226.

- [60] CMS Collaboration, “CMS Luminosity Measurement for the 2016 Data Taking Period”, CMS Physics Analysis Summary CMS-PAS-LUM-17-001, CERN, 2017.
- [61] J. Butterworth et al., “PDF4LHC recommendations for LHC Run II”, *J. Phys. G* **43** (2016) 023001, doi:10.1088/0954-3899/43/2/023001, arXiv:1510.03865.
- [62] T. Junk, “Confidence level computation for combining searches with small statistics”, *Nucl. Instrum. Meth. A* **434** (1999) 435, doi:10.1016/S0168-9002(99)00498-2, arXiv:hep-ex/9902006.
- [63] A. L. Read, “Presentation of search results: The  $CL_s$  technique”, *J. Phys. G* **28** (2002) 2693, doi:10.1088/0954-3899/28/10/313.
- [64] ATLAS and CMS Collaborations, “Procedure for the LHC Higgs boson search combination in summer 2011”, Technical Report ATL-PHYS-PUB-2011-11, CMS-NOTE-2011-005, CERN, 2011.
- [65] B. Fuks, M. Klasen, D. R. Lamprea, and M. Rothering, “Gaugino production in proton-proton collisions at a center-of-mass energy of 8 TeV”, *JHEP* **10** (2012) 081, doi:10.1007/JHEP10(2012)081, arXiv:1207.2159.
- [66] B. Fuks, M. Klasen, D. R. Lamprea, and M. Rothering, “Precision predictions for electroweak superpartner production at hadron colliders with RESUMMINO”, *Eur. Phys. J. C* **73** (2013) 2480, doi:10.1140/epjc/s10052-013-2480-0, arXiv:1304.0790.
- [67] B. Fuks, M. Klasen, D. R. Lamprea, and M. Rothering, “Revisiting slepton pair production at the Large Hadron Collider”, *JHEP* **01** (2014) 168, doi:10.1007/JHEP01(2014)168, arXiv:1310.2621.